LBL-18751
UC-11

Lawrence Berkeley Laboratory
UNIVERSITY OF CALIFORNIA

APPLIED SCIENCE DIVISION

FY 1984 Annual Report

CHEMICAL PROCESS RESEARCH AND DEVELOPMENT PROGRAM

July 1985

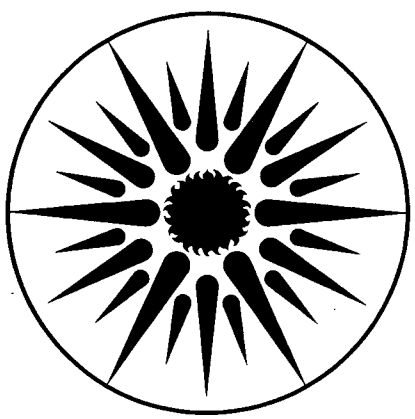

APPLIED SCIENCE DIVISION

Prepared for the U.S. Department of Energy under Contract DE-AC03-76SF00098

DISCLAIMER

LBL-18751

APPLIED SCIENCE DIVISION ANNUAL REPORT

CHEMICAL PROCESS RESEARCH & DEVELOPMENT PROGRAM

FY 1984

Elton J. Cairns
Program Leader
Head, Applied Science Division
and
Associate Director, LBL

Applied Science Division
Lawrence Berkeley Laboratory
University of California
Berkeley, California 94720

Prepared for the U.S. Department of Energy under Contract No. DE-AC03-76SF00098

CONTENTS

CHEMICAL PROCESS RESEARCH AND DEVELOPMENT PROGRAM STAFF

Elton Cairns, Program Leader
Harvey Blanch, Deputy Program Leader

Thomas Adler
El-Sayed Arafat
Daniel Arenson
Myra Baker
Frann Bell
Wyn Bennett
Paul Berdahl
Douglas Bousfield
Garth Burns
Van Carey
Grace Chou
Yew Khoy Chuah
Robert Demyanovich
Morton Denn
Minh Do
Jesse Dobson
Gregory Dow
Richard Fish
John Fitch
James Flatt
Loree Fowell
Robert Goldberg
Terry Grant
Edward Grens
Donald Hanson
Richard Hix
Arlon Hunt
Mark Isaacson
Alejandro Izquierdo
Rajiv Jain
Eileen Keefe
Aviezer Kertes
Tae-Jeong Kim
C. Judson King
Kim Kinoshita
John Komlenic
Susan Lauer
Phillip Lessner
Gary Lipscomb
Scott Lynn
Patricia Mackenzie
Brian Maiorella
Giuseppe Marrucci
Frank McLarnon
Kenneth Miller
Curtis Munson
Stewart Naftel
Joann Nakamura
Timothy Oolman
Rollie Otto
Kenneth Purcell
William Rixey
Ricardo San Martin
Michael Schuh
Aldo Sciamanna
Steve Sciamanna
John Senetar
Michael Smith
Craig Stevens
Kathy Striebel
Jon Sundquist
Janet Tamada
Raja Tannous
Rodney Thompson
Arne Thormodsen
Kent Udell*
Theodore Vermeulen
Dale Wiley
Charles Wilke
Brian Wines
Jack Winnick†

*Earth Sciences
†Participating guest.

CHEMICAL PROCESS RESEARCH AND DEVELOPMENT PROGRAM

INTRODUCTION

The Chemical Process Research and Development Program has five main projects applying chemistry and chemical engineering to problems in the production of new fuels, their environmental impact, and energy storage. These projects are:

(a) Organometallic geochemistry
(b) Processing of effluent gases and liquids resulting from synthetic-fuel production, to provide acceptable waste or recycle streams
(c) Production of liquid fuels from biomass
(d) Electrochemical energy storage
(e) Thermal energy storage

Each of these projects focuses on transport-process principles, chemical kinetics, thermodynamics, separation processes, and organic and physical chemistry.

The first project involves the removal of metal compounds from the complex chemical matrices that make up fossil-fuel precursors and products. Such removal is important for efficient refining and for environmental protection. Accordingly, LBL has developed a program to molecularly characterize these organometallic and inorganic complexes. The program is also developing innovative methods to remove these compounds by using model ligands for future polymer-supported analogues.

The second project involves the development of novel and improved methods for processing synfuel condensate waters to make them suitable for recycle, thereby minimizing process-water requirements. The main emphasis is on physiochemical methods, particularly solvent extraction and stripping, to remove organics. Identification of the contaminating organics is difficult, but necessary to permit development of appropriate solvents for their removal. LBL studies have successfully examined simultaneous solvent extraction in removal of ammonia and acid gases by stripping.

The conversion of biomass to liquid fuels has been an area of considerable research and development within the Chemical Process Program over the past several years. The biological conversion of wood and agricultural residues to ethanol has been examined. An enzymatic hydrolysis of these cellulosic materials has been developed to yield monomeric hexose and pentose sugars. These can be subsequently fermented to produce ethanol. Various high-rate fermentation processes have been developed, and novel processes for ethanol recovery that are less energy intensive than conventional processes are being studied.

The electrochemical energy storage program provides research to develop advanced battery systems for electric vehicle and stationary energy storage applications. Topics include identification of new electrochemical couples for advanced batteries, determination of technical feasibility of the new couples, improvements in battery components and materials, establishment of engineering principles applicable to electrochemical energy storage and conversion, and the assessment of fuel-cell technology for transportation. Major emphasis is on applied research that will lead to superior performance and lower life-cycle costs.

The fifth project is a series of research and development efforts in thermal energy storage. This project focuses on new and innovative approaches that have a broad range of applications and on the utilization of solar energy.

Production of Sugars from Cellulose: The Kinetics of Endoglucanase in Cellulose Hydrolysis*

B. Elzufon, D. Wiley, H. Blanch, C. Wilke, and A. Sciamanna

The research of the Biochemical Process Group has focused on the hydrolysis of lignocellulosic materials to sugars and their subsequent fermentation by yeast to ethanol and other fuel-grade chemicals. Various studies have examined the kinetics of enzymatic hydrolysis of cellulose and hemicellulose fractions for optimal sugar production, the physical and chemical nature of the raw materials, the optimal production and recovery of enzymes, and the use of new organisms for converting polymeric pentosans and hexosans to sugars.

Cellulase is composed of three individual enzymes that function synergistically to break down cellulose. An overall kinetic model of cellulase behavior is being developed based on models of the behavior of the individual enzymes. In this article, an effort to develop a kinetic model of endoglucanase, one of the three cellulase enzymes, is reported.

ACCOMPLISHMENTS DURING FY 1984

A modified viscometric technique was developed to assay endoglucanase activity and was used to determine its kinetic parameters. Endoglucanase was found to be more active in its pure form than as part of the cellulase system. This may be due to the accumulation of cellobiose, a product of cellobiohydrolase, which inhibits endoglucanase. The influence on endoglucanase activity of cellobiose and glucose, known inhibitors of cellulase, was also studied. Cellobiose was found to inhibit endoglucanase via partial mixed-type inhibition. Glucose, however, was found to be a nonessential activator of endoglucanase.

An analytical technique was developed to measure enzyme activity that takes advantage of the polymeric characteristics of cellulose. Once developed, this technique was used to study endoglucanase behavior. A kinetic model was then developed based on experimentally determined kinetic parameters. An additional model based on these inhibition and activation mechanisms was developed and was successful in predicting endoglucanase behavior.

A typical single polymeric carbohydrate component from biomass contains molecules of many different chain lengths. A molecular weight measure will therefore yield only an average value. There are three methods of averaging the molecular weight of different polymer chains in a mixture: (1) a molecule-number average molecular weight, M_n; (2) a weight average molecular weight, M_w; and (3) a viscosity average molecular weight, M_v.

M_n is determined by counting the number of molecules in a sample of a given weight and determining the average weight on the basis of the number of molecules at each weight. Molecular weights can be measured by determining the number of molecules in a sample of known weight by chemically reacting the end groups with some compound so that they can be distinguished from the other monomer units. An example is the colorimetric reaction.[1] This method of molecular weight determination is also the basis for the reducing sugar assay. M_n is usually the most probable molecular weight and lies near the peak of a molecular weight distribution curve, as shown in Fig. 1.

M_w determines average molecular weight by the weight percent of each molecule present. The ratio of M_w to M_n is a measure of the range of the molecular weight distribution and is called the polydispersity; for carboxymethyl cellulose (CMC), polydispersity is assumed to be two.[2]

M_v is determined by relating molecular weight to solution viscosity and is the simplest experimental method for measuring the molecular weight of a polymer. It lies between M_n and M_w and is usually closer to M_w, as shown in Fig. 1. Since M_v is close to M_w it is approximately equal to M_w; therefore, $M_v \approx M_w \approx 2M_n$. Thus the viscosity method for assaying endoglucanase activity is also the basis for measuring the molecular weight of a polymer.

*This work was supported by the Office of Energy Research, Office of Basic Energy Sciences, Chemical Sciences Division of the U.S. Department of Energy under Contract No. DE-AC03-76SF00098 and by the Solar Energy Research Institute under Contract No. DX-4-04059-1.

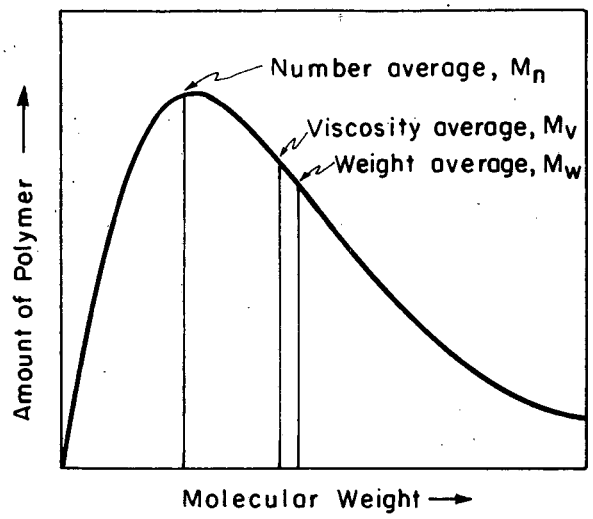

Figure 1. Molecular weight distribution of a typical polymer.[3] (XBL 839-6385)

M_v is related to the intrinsic viscosity of a polymer by the Mark-Houwink equation:

$$[\eta] = H(M_v)^x \quad , \tag{1}$$

where H and x are constants and $[\eta]$ is the intrinsic viscosity.[3] Intrinsic viscosity is a physical property of the polymer and is defined as a measure of the polymer's ability to increase the viscosity of a solvent in the absence of polymer-polymer interaction or at infinite dilution.[2] The relationship between viscosity and concentration that is most suited to CMC is the Baker relation:

$$\frac{\eta}{\eta_s} = \left(1 + \frac{[\eta]}{C_s}\right)^8, \tag{2}$$

where η_s is the solvent viscosity and η is the solution viscosity.[2] The Baker relationship is only valid for polymer solutions of low concentration.

This method of molecular weight determination is applied to the viscometric assay by measuring the viscosity change in a dilute solution with time once the enzyme has been added. Viscosity is related to M_n by the relation:

$$\eta \underset{(a)}{\longrightarrow} [\eta] \underset{(b)}{\longrightarrow} M_v \underset{(c)}{\longrightarrow} M_n \quad ,$$

where (*a*) is Eq. (2), (*b*) is Eq. (1), and (*c*) is the polydispersity.

CMC was used as a substrate for all the kinetic experiments; it is a cellulose ether produced by reacting alkali cellulose with sodium monochloracetate. Its structure is close to that of cellulose except that, on some of the monomer units, a carboxymethyl group ($-OCH_2COO^-$) is substituted for the hydroxyl group attached to the sixth carbon. While structurally similar to cellulose, CMC is water soluble. Therefore, it can be used to examine the kinetic behavior of endoglucanase or cellulase on long polymer chains.

The CMC used was medium viscosity; obtained from Sigma Chemical (No. C-4888), it had a reported viscosity average molecular weight of 250,000 daltons, an average degree of polymerization of 1100, and a degree or substitution of 0.7. The molecular weight of this lot of CMC ranged from 130,000 to 250,000 daltons as determined viscometrically. The CMC was dissolved in 0.05 *M* sodium acetate buffered to a pH of 5.0. The polydispersity was assumed to be two, and the Mark-Houwink constants from Eq. (1) were $H = 2.17 \times 10^{-5}$ and $x = 0.83$ (Ref. 2).

At low concentrations, CMC solutions are Newtonian fluids, but, at higher concentrations, they exhibit power-law behavior. For the kinetic experiments done in this study, the solution concentrations ranged from 10 to 30 g/L. The rheological behavior of CMC in this range is summarized in Table 1. In the concentration range used, CMC behaved as a power-law fluid. For the inhibition experiments, glucose and cellobiose were also added to the solutions, which did not affect the rheological behavior of the solution.

The mutant strain of *Trichoderma reesei*, Rutgers-C30, produced the cellulase enzyme used in this study. Endoglucanase and cellobiohydrolase are extracellular enzymes, while β-glucosidase is primarily cell-bound.[4] The fermentation broth was ultrafiltered with 0.005 *M* ammonium carbonate and concentrated to 238 grams of soluble protein per

Table 1. Rheology of concentrated, medium-viscosity CMC.

M_v (dalton)	CMC (g/L)	K[a] (P/sec)	n[a]	η_{app}[b] (cp)
280,000	10	0.816	0.87	37.4
250,000	30	41.7	0.65	512
	20	5.54	0.78	148
	10	0.424	0.89	21.9
130,000	30	5.47	0.80	165
	20	1.18	0.86	51.0

[a] $\tau = K(D)^n$, where τ is shear stress and D is shear rate.
[b] $\eta_{app} = K(D)^{n-1}$ for $D = 400\ sec^{-1}$.

liter.[5] The raw cellulase had specific endoglucanase activity of 6.0 units per mg of soluble protein and a specific β-glucosidase activity of 2.6 units per mg. A unit of activity is the micromoles of bonds broken or micromoles of reducing sugars produced per minute when an appropriate substrate is enzymatically reacted.

The cellulase was fractionated using ion exchange chromatography,[5] and seven separate peaks were collected. The results of the typical ion exchange are shown in Table 2. Fractions II and V showed significant endoglucanase activity. Fraction II was a low molecular weight protein that also had β-glucosidase activity. Fraction V was a high molecular weight protein with a very low β-glucosidase activity, approximately 96% pure endoglucanase, used in this study. Gel electrophoresis showed it to have two components. The major component had a molecular weight of approximately 66,000, and the minor component had a molecular weight of approximately 29,000. Each enzyme component obtained in the ion exchange was purified further by gel permeation chromatography (GPC). Fraction V-A was shown to be pure protein via gel electrophoresis, and it had a specific endoglucanase activity of 25.4 U/mg. The other peak, V-B, was also high in endoglucanase activity with a specific activity of 10.2 U/mg.

In order to correlate viscosity with intrinsic viscosity, and thus with molecular weight, it was necessary to obtain samples covering a range of molecular weights typical of those found over the assay reaction period. This was done by adding varying amounts of cellulase to a polymer solution and allowing the reaction to take place at 40°C for 5 minutes. The reaction was quenched by increasing the pH of the solution to 10, temporarily deactivating the enzyme. The cellulase was then denatured by heating the solution to 90°C for about 5 minutes, and the solution was returned to its original pH of 5.

Samples of different molecular weights were prepared this way, and the apparent viscosity of each sample was determined at the high substrate concentrations. Each sample was then diluted and its intrinsic viscosity measured. Correlation curves were developed in this manner for 10, 20, and 30 g/L CMC solutions. The relationships developed were used to correlate viscosity, η, to intrinsic viscosity, $[\eta]$, and were of the form,

$$[\eta] = a + b\eta \quad . \tag{3}$$

The values of a and b that were determined are listed in Table 3. These correlations are considered valid for CMC solutions of number average molecular weights ranging from 50,000 to 130,000.

A Couette viscometer was used to measure the rheology of the concentrated solutions, and a capillary viscometer was used to measure the viscosity of the dilute solutions. The assay, when performed in a Couette viscometer, was at a constant shear rate for the entire reaction period. The original viscosity of the CMC solution was measured, cellulase or endoglucanase was added to the solution, and the solution was returned to the viscometer. Viscosity change was measured with respect to time by measuring the change in torque with respect to time at a constant shear rate. A typical degradation curve is shown in Fig. 2. The reaction progress was recorded in this manner for approximately 5 minutes or until the viscosity change became very small. All assays were performed at 40°C, which is near the optimum tem-

Table 2. Cellulase enzyme description.

Cellulase fraction	Wt.% of total soluble protein	β-Glucosidase activity (U/mg)		Endoglucanase activity (U/mg)	
		ion exch.	gel perm.	ion exch.	gel perm.
Total cellulase	100.0	2.6		6.0	
I-A	10.1	27	146.0	0.32	1.0
I-B			7.3		0.4
II	31.0	4.2	0.2	16.0	27.2
III	17.3	0.03	0.05	1.3	3.7
IV	8.0	0.03	0.03	0.74	0.78
V-A	8.3	0.04	0.04	24.8	25.4
V-B	0.3		0.03		10.2
VI	11.4	0.05	0.09	1.6	5.0
VII	13.9	0.01	0.0	0.53	0.29

Source: Ref. 5.

Table 3. Parameters for viscosity–intrinsic viscosity correlation for medium viscosity carboxymethylcellulose.

CMC (g/L)	a[a]	b[a]
10	0.251	1.40×10^{-2}
20	0.254	2.51×10^{-3}
30	0.257	6.04×10^{-4}

[a]Parameters fitting Eq. (3).

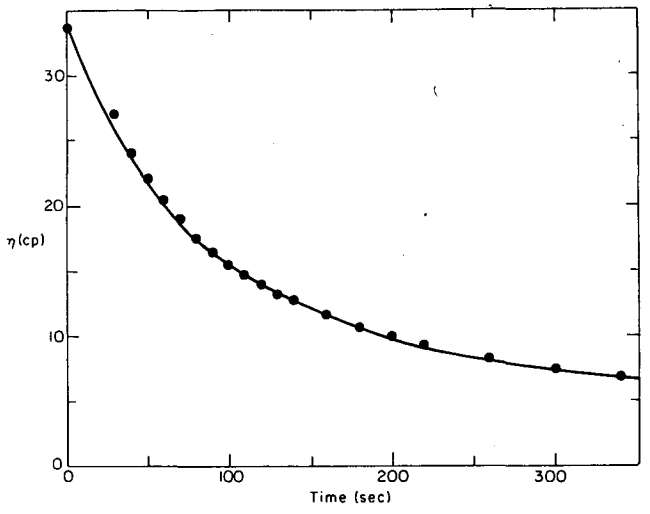

Figure 2. Effect of enzymatic degradation on solution viscosity. (XBL 839-6388)

perature of 45°C for cellulase activity and is consistent with kinetic experiments carried out by others.[2] Activity was determined from the slope of the linear portion of a plot of $1/M_n$ versus time according to Eq. (1). A typical plot is shown in Fig. 3. Activity was measured as a function of substrate concentration for different enzyme concentrations, and inhibition parameters were then determined for cellulase and endoglucanase. At a constant enzyme concentration, activity was measured at different cellobiose concentrations; these experiments were repeated using glucose. In order to determine the type of inhibition present, experiments were performed in which both glucose and cellobiose were added to the reaction mixture.

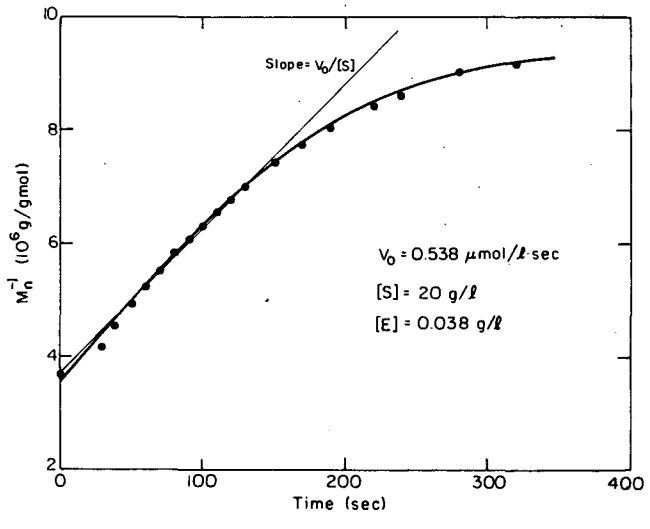

Figure 3. Activity determination for endoglucanase. (XBL 839-6389)

The kinetic parameters describing the behavior of endoglucanase were determined from experimental data. First, the effect of enzyme concentration on reaction velocity, v_o, was examined. Second, the role of glucose in endoglucanase regulation along with the effect of cellobiose on endoglucanase activity was considered. Third, the behavior of purified endoglucanase was compared to the behavior of endoglucanase in the presence of the other cellulolytic enzymes. Using initial rate models for activation and inhibition, kinetic parameters were fit to the data and incorporated into an overall model of endoglucanase behavior.

An assumption of Michaelis-Menten kinetics[6] is that the reaction velocity is directly proportional to the concentration of the enzyme substrate complex,

$$v_o = k_p[ES] \quad . \tag{4}$$

It then follows that the maximum reaction velocity is proportional to the total enzyme concentration,

$$V_{\max} = k_p[E_t] \quad , \tag{5}$$

where k_p is the rate constant for the product-forming step. Lineweaver-Burk plots were prepared for various enzyme concentrations, and $V_{\max}$ was determined at each concentration for both cellulase and endoglucanase. In the range of enzyme concentrations tested, $V_{\max}$ was a linear function of E_t as can be seen in Figs. 4 and 5.

The advantages of the Couette viscometric technique are that it can measure initial rates and allows the use of higher enzyme and substrate concentrations. On the basis of the consistency of the results of the kinetic studies, it is an effective method for studying initial rate kinetics. However, it is limited for the study of reaction progress versus time because the molecular weight distribution and how it changes with time is not known. If the initial value of the polydispersity can be determined exactly, then the assay can measure absolute activities rather than relative values.

While the $V_{\max}$ values may be slightly inaccurate, the values of the Michaelis constant and the inhibition and activation parameters will not be affected by a change in the value used for k. A serious limitation of the assay is that the dependence of the molecular weight distribution on time must be determined concurrently, such as with GPC.

Endoglucanase activity was evaluated assuming that Michaelis-Menten kinetics could be applied under the given experimental conditions. The assumptions on which the Michaelis-Menten model are based appear to be reasonable for the experimen-

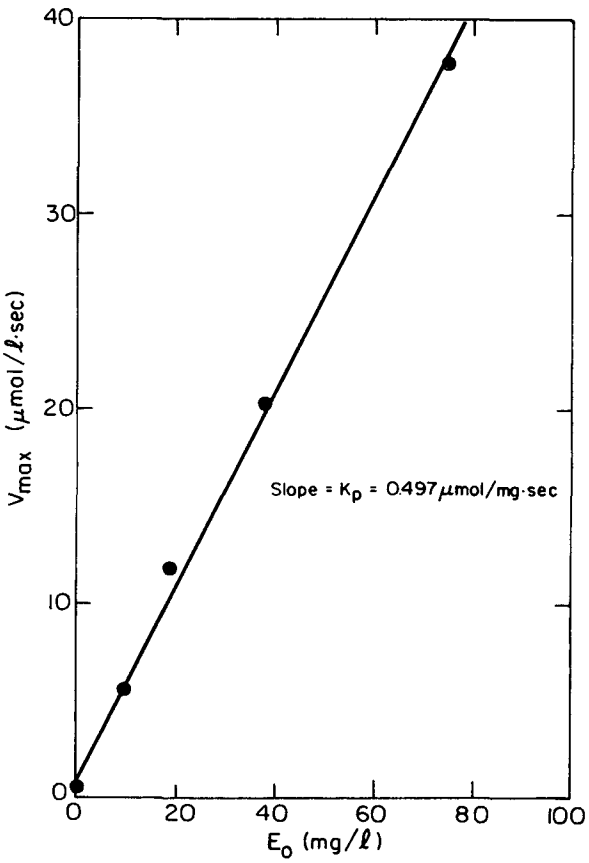

Figure 4. Determination of k_p for cellulase.
(XBL 839-6390)

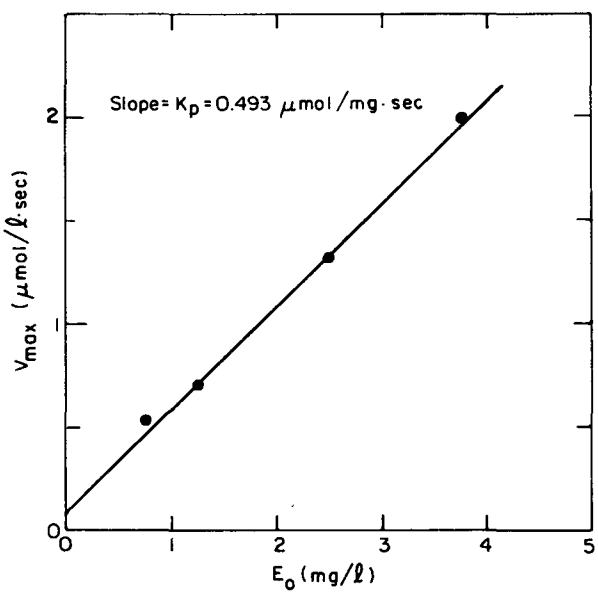

Figure 5. Determination of k_p for endoglucanase.
(XBL 839-6391)

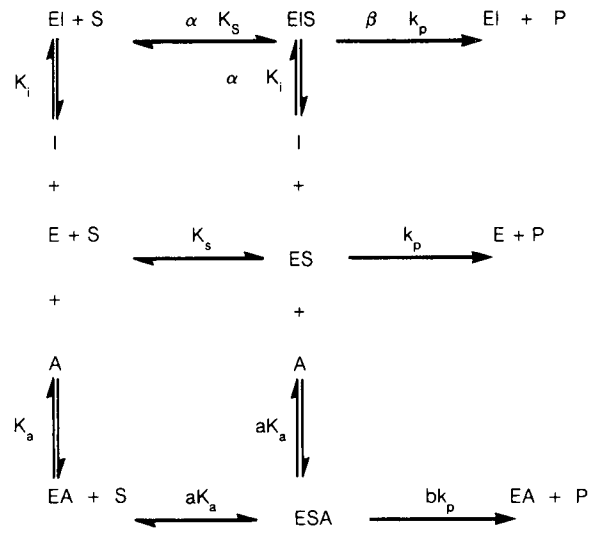

Figure 6. Schematic model of endoglucanase behavior: A nonessential activator in competition with a partial mixed-type inhibitor. (XBL 8311-4474)

tal conditions in this study. One of these assumptions is that V_{max} is directly proportional to the total enzyme concentration. As can be seen in Figs. 4 and 5, a linear enzyme dilution curve was obtained. Glucose and cellobiose have been identified as inhibitors of the cellulase system. Their effect on endoglucanase was studied. Cellobiose was found to inhibit endoglucanase via a partial mixed-type inhibition mechanism. Glucose, on the other hand, was found to be a nonessential activator of endoglucanase. The overall model of endoglucanase behavior can be represented schematically by Fig. 6. This is a model of a nonessential activator in competition with a partial mixed inhibitor. The values of the kinetic parameters for this model are summarized in Table 4.

Table 4. Kinetic parameters for endoglucanase activity.

	Cellulase	Endoglucanase
K_m	0.030	0.028
K_i	0.012	0.004
α	1.26	1.70
β	0.572	0.606
K_a	2.00	0.250
a	0.468	0.470
b	2.21	1.15

PLANNED ACTIVITIES FOR FY 1985

The results reported here will be incorporated into an overall model for the cellulase system of enzymes derived from the *T. reesei* mutant strain Rut-C30.

REFERENCES

1. Orichowskyj, S.T. (1982), "Recovery of Cellulase Enzymes by Countercurrent Adsorption," M.S. Thesis, University of California, Berkeley.
2. Almin, K.E., and Eriksson, K.E. (1967), "Enzymic Degradation of Polymers (I), Viscometric Determination of Enzymic Activity," *Biochim. Biophys. Acta. 139*, p. 248.
3. Billingham, N.C. (1977), in *Molar Mass Measurement in Polymer Science,* Wiley and Sons, New York.
4. Ghose, T.K. (1977), in *Advances in Biochemical Engineering,* Vol. 6, p. 39, T.K. Ghose, A. Fiechter, and N. Blakebrough, Eds., Springer-Verlag, Berlin.
5. Wiley, D. (1985), *Mechanism and Kinetics of Cellulose Hydrolysis,* Ph.D. Thesis, University of California, Berkeley.
6. Segel, I.H. (1975), in *Enzyme Kinetics,* Chapters 3–5, Wiley and Sons, New York.

Production of Sugars from Cellulose: Cellulase Production by *T. Reesei* in Continuous Culture in Lactose Medium*

F. Castillo, H. Blanch, and C. Wilke

In the process of cellulose utilization, perhaps the most obvious area for major improvement is the production of cellulase enzyme for hydrolysis of wood and agricultural residues that can then be fermented into ethanol fuel. Nearly 50% of the cost of producing glucose from cellulosic material is attributed to enzyme production alone. Improvements in this step would therefore have dramatic impact and are important if economical hydrolysis processes are to be realized.

The first major thrust in this area has been the development of improved mutant strains of the filamentous fungus *Trichoderma reesei*, free from catabolite repression and capable of constitutive cellulase production. One such hyperproducing mutant, developed at Rutgers University (Rut-C30) and isolated,[1] presents an interesting potential for the development of processes aimed at the commercial production of cellulases.

Lactose is utilized by this microorganism; when it grows on this disaccharide, the enzymes of the cellulase complex are induced. This fact suggests that milk or cheese whey may be used as a medium to grow Rut-C30 and produce the enzymes. This procedure may also be an efficient method of whey treatment, reducing its high biological oxygen demand (BOD).[2,3] Additional advantages of whey utilization are its solubility and ease of handling as a fermentation medium compared to insoluble cellulose and its rich composition in nutrients[4,5] that may require only a few economical supplementations.

ACCOMPLISHMENTS DURING FY 1984

The objectives of this work are twofold: (1) to obtain information on the regulatory controls operating on the synthesis of the cellulases and (2) to study the effects of environmental variables on the production of the enzymes.

Rut-C30 strain was used throughout the experiments. The fermentation medium consisted of a double concentration of salt solution modified from that of Ryu *et al.*[6] to insure lactose limitation. It contained per liter: 25 g lactose, 4 g $(NH_4)_2(SO_4)$, 2 g KH_2PO_4, 0.3 g $MgSO_4 \cdot 7\ H_2O$, 0.15 g $CaCl_2 \cdot 2H_2O$, and 0.2 mL surfactant (Tween 80). For foam control, General Electric silicon AF-60 at 0.05 to 0.1 v/v% was used. For continuous culture, a Chemap 20 L fermentor was used, with a 5 L reactor vessel (2.5 to 2.8 L working volume). Regulation of pH was carried out by automatic addition of 2 *N* ammonium hydroxide.

After samples were withdrawn aseptically from the reactor vessel, they were divided into two fractions: one was frozen whole while the second was filtered through 0.45 micrometer polycarbonate membranes, with the filtrate frozen until it was assayed. Assays for enzyme activities included deter-

*This work was supported by the Assistant Secretary for Conservation and Renewable Energy of the U.S. Department of Energy under Contract No. DE-AC03-76SF00098 and by the Solar Energy Research Institute under Contract No. DR-0-9058-1.

minations of filter paper activity, endoglucanase (CMCase), and cellobiohydrolase (cotton activity) by methods described previously[7]; cellobiase (β-glucosidase) and lactase (β-galactosidase) were assayed with p-nitrophenyl glucopyranoside (p-NPG) and o-nitrophenyl galactopyranoside as substrates, respectively, at 5 m*M* final concentrations. Activities of both enzymes as functions of temperature and pH indicated that, for cellobiase activity determined with p-NPG, the optimum pH was 4.6 and the optimum temperatures were 73°–75°C. For lactase activity, they were 4.6 and 62°–65°C, respectively.

The organism is a complete prototroph and grew well in this simple medium. Dry weight, intra- and extracellular protein, and total biomass (dry weight and extracellular protein) as functions of dilution rate are shown in Figs. 1 and 2. As can be seen, reduction of antifoam concentration from 0.1 to 0.05% produced slight increases in the cellular protein. In this medium, the maximum yield obtained was 0.486 g total biomass/per gram lactose utilized, and the maintenance coefficient was calculated at 6 mg lactose per gram of total biomass per hour. Maximum specific growth rate was 0.12 per hour, and the saturation constant for lactose was estimated at 0.763 g/L (0.77 m*M*).

The profiles of enzyme production and specific activities as functions of dilution rate when the medium contained 0.1% antifoam are shown in Figs. 3 and 4. In subsequent experiments, antifoam was not added and the foam was easily kept under control by reducing the aeration rate. The profiles obtained for production of the enzyme (Fig. 3) indi-

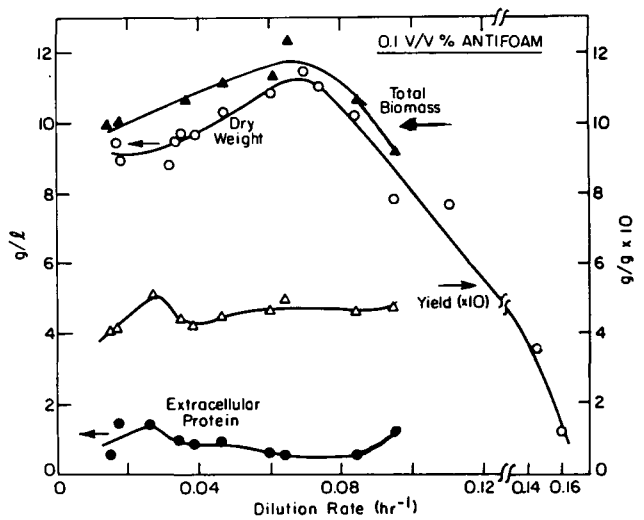

Figure 1. Various parameters of Rut-C30 growth in submerged culture vs. substrate (lactose) dilution rate in the presence of 0.1 v/v% antifoam. (XBL 8311-6604)

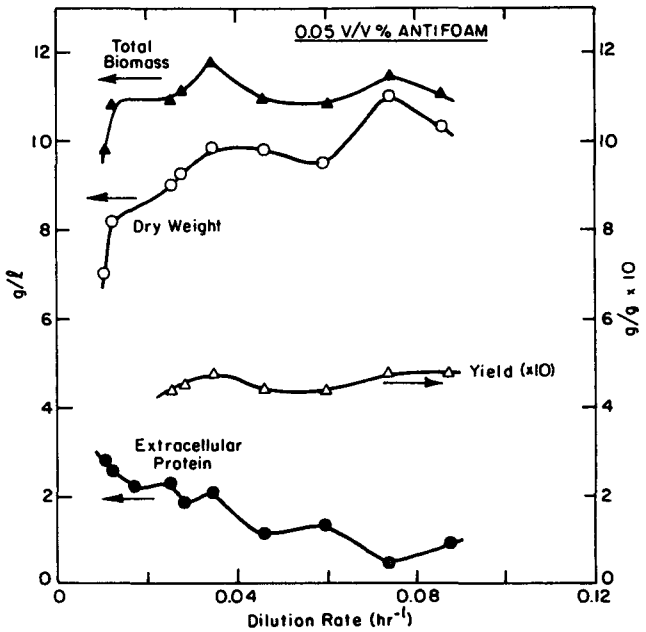

Figure 2. Various parameters of Rut-C30 growth in submerged culture vs. lactose dilution rate in the presence of 0.05 v/v% antifoam. (XBL 8311-6605)

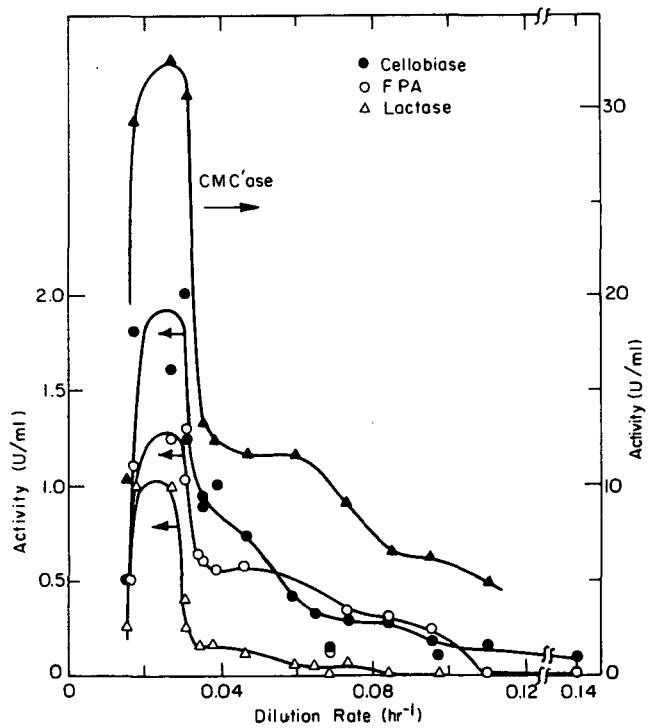

Figure 3. Growth profiles of enzyme components vs. dilution rate in the presence of 0.1 v/v% antifoam. (XBL 8311-6606)

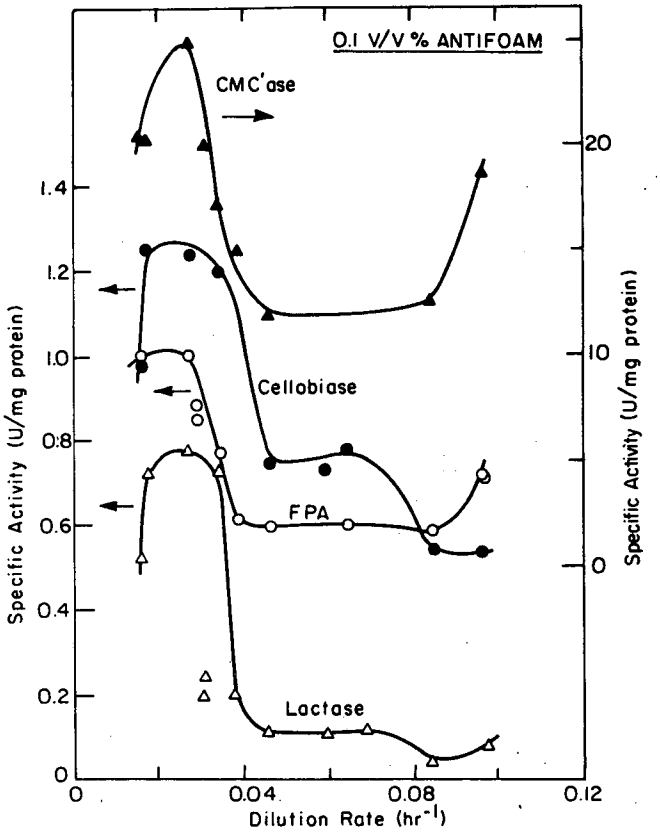

Figure 4. Specific growth profiles of enzyme components vs. dilution rate in the presence of 0.1 v/v% antifoam.
(XBL 8311-6607)

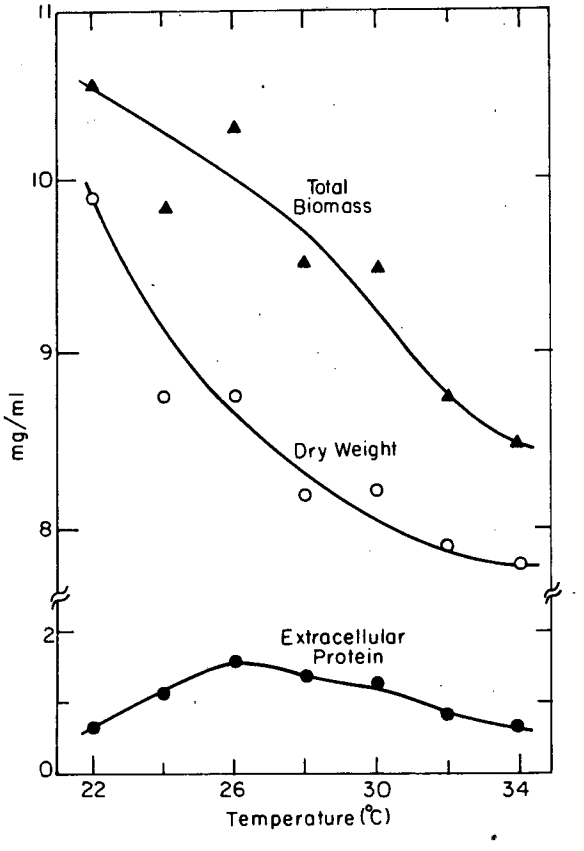

Figure 5. Steady-state growth of Rut-C30 vs. temperature.
(XBL 8311-6608)

cate the presence of dual regulatory mechanisms for the synthesis of the enzymes, their induction, and catabolite repression.[8]

The organism was found to produce a lactase, and the activity of this enzyme was assayed only in the filtrates. Although the enzyme was present outside of the cell, no significant levels of glucose were detected in the medium even at high dilution rates. This lactase may be excreted by the organism along with the other enzymes, or its presence in the medium may result from cell lysis or fragmentation caused by the high-speed agitation, or both.

To study the effects of temperature and pH on the production of the enzymes, the dilution rate was fixed. One parameter was varied at a time, and the new steady states were allowed to stabilize after each variation. Figures 5, 6, 7, and 8 show the steady-state values for biomass, protein, and enzymes as functions of temperature and pH.

For the next set of experiments, 26°C and pH 5 were selected and maintained. To study the effects of nutrient addition, pulses (equivalent to 1% of working volume) were added to the reactor vessel

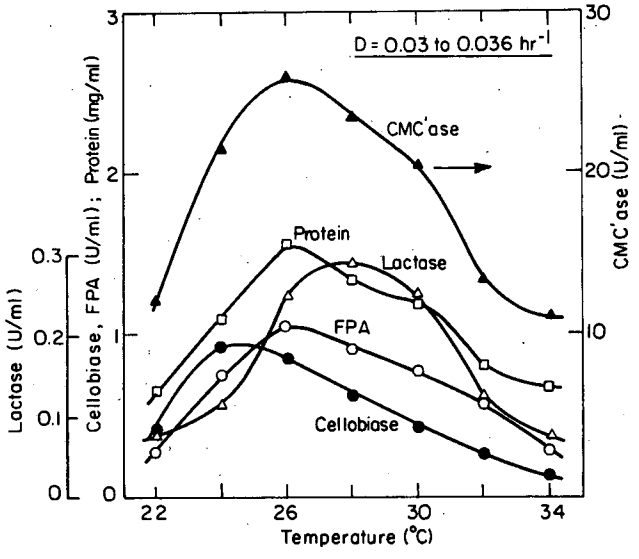

Figure 6. Growth profiles of enzyme components vs. temperature at dilution rates of 0.03 to 0.036 hr^{-1}.
(XBL 8311-6609)

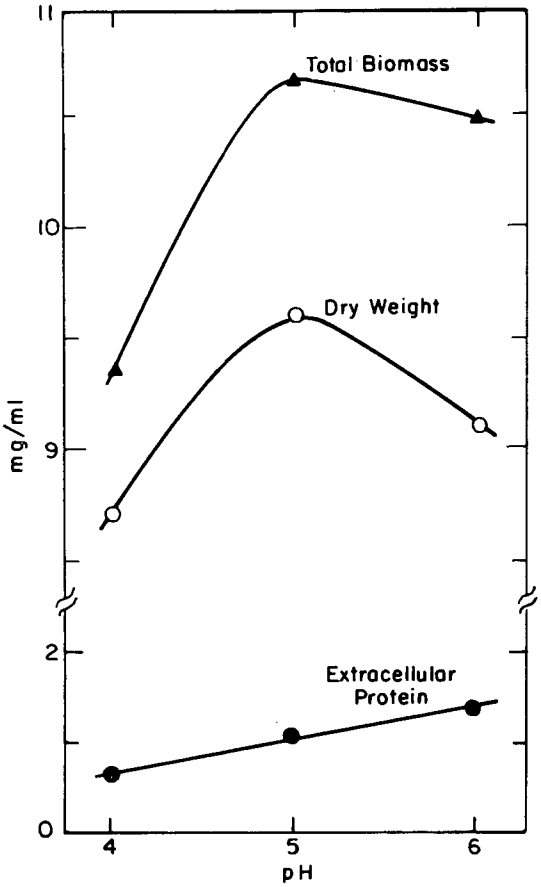

Figure 7. Steady-state growth of Rut-C30 vs. pH.
(XBL 8311-6610)

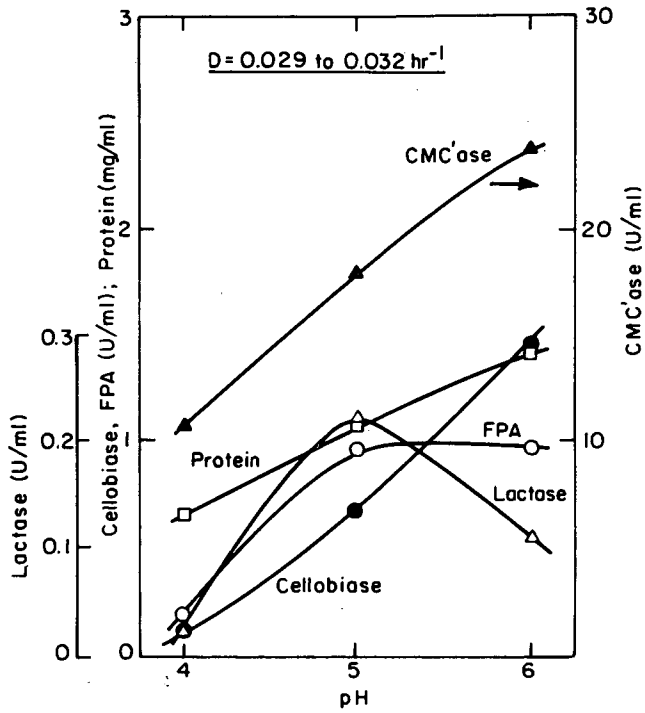

Figure 8. Growth profiles of enzyme components vs. pH at dilution rates of 0.029 to 0.032 hr^{-1}.
(XBL 8311-6611)

and the responses studied with respect to time. Addition of a yeast nitrogen base (YNB) pulse at 50 times the standard concentration produced increases in all of the enzymes (Fig. 9). When pulses of glucose or lactose were applied, transient decreases in the levels of all five enzymes were observed, such as would occur in catabolite repression. When the different groups of nutrients from YNB were tested separately, none induced the observed increase in enzyme productivity as when whole YNB was used.

Addition of the surfactant Tween 80 did increase the levels of the enzymes. Other nutrients and compounds used in the past, such as urea, proteose peptone, or corn-steep liquor, did not enhance enzyme levels. When the medium was shifted to 2 times the standard concentration, the original transient decrease in all enzymes was followed by an increase to new high levels.

PLANNED ACTIVITIES FOR FY 1985

Capital and energy costs concentrate in the enzyme production step of the biomass hydrolysis process. When steam-exploded wood is used as the cellulose source, in the overall process, about 12% of the total input is used in enzyme production. Process economic evaluation indicates that the use of

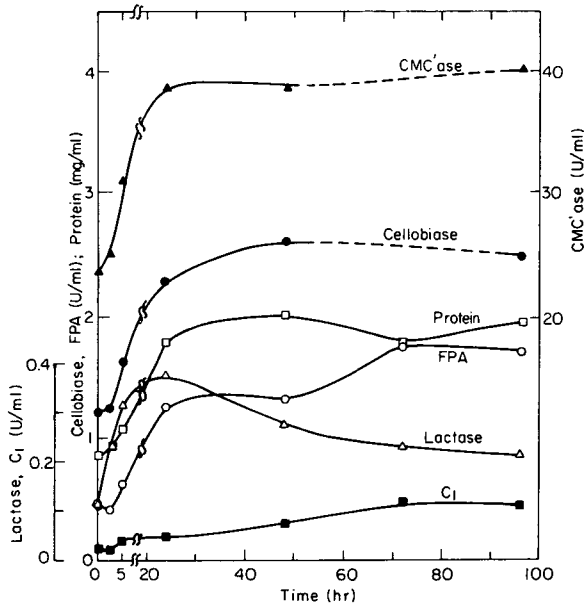

Figure 9. Growth of enzyme components over time with added yeast nitrogen base, 30 mL, 50× standard concentration. (XBL 8311-6612)

delignified or soluble carbon sources such as lactose in whey is favorable in fed-batch or continuous cultivation, respectively. The optimum conditions for the initial batch period using this substrate will be determined. The effect of feeding regimes and aeration conditions on enzyme production will be studied. Experiments in which application of pulses with combinations of different groups of nutrients and use of a more concentrated medium are contemplated.

REFERENCES

1. Montenecourt, B.S. and Eveleigh, D.E. (1977), "Preparation of Mutants of *T. reesei* with Enhanced Cellulase Production," *Appl. Environ. Microbial. 34*, p. 777.
2. Kosikowski, F.V. (1977), *Cheese and Fermented Milk Foods,* Edward Brothers, Inc., Ann Arbor, Michigan.
3. Wix, P. and Woodbine, M. (1958), "The Disposal and Utilization of Whey; a Review," *Dairy Sci. Abstracts 20*, p. 537, Part 1; p. 621, Part 2.
4. Mairopoulou, I.P. and Kosikowski, F.V. (1972), "Composition, Solubility and Stability of Whey Powders; Free Amino Acids and Soluble Peptides of Whey Powders," *J. Dairy Sci. 56*, p. 1128, Part 1; p. 1135, Part 2.
5. Glass, L. and Hedrick, T.I. (1977), "Nutritional Composition and Major Factors Including Amino Acids in Sweet and Acid Type Dry Wheys; Vitamins, Mineral and Calorie Contents of Dry Wheys," *J. Dairy Sci. 60*, p. 185, Part 1; p. 190, Part 2.
6. Ryu, D., Andreotti, R., Mandels, M., Gallo, B., and Reese, E.T. (1979), "Studies on Quantitative Physiology of *Trichoderma reesei* with Two-Stage Continuous Culture for Cellulase Production," *Biotechnol. Bioeng. 21*, p. 1887.
7. Wilke, C.R. and Blanch, H.W. (1981), *Bioconversion of Cellulose,* LBL-14219.
8. Toda, K. (1981), "Induction and Repression of Enzymes in Microbial Culture," *J. Chem. Tech. Biotechnol. 31*, p. 775.

Molecular Characterization of Vanadium and Nickel Non-Porphyrin Compounds Isolated from Heavy Crude Petroleums*

R.H. Fish, A. Izquierdo, J.J. Komlenic, J.G. Reynolds,† and E.J. Gallegos†

Recently, we have found, using reverse-phase high-performance liquid chromatography–graphite-furnace atomic absorption (RP-HPLC-GFAA), that highly polar non-porphyrin nickel compounds are extracted with pyridine/water from Wilmington petroleum, as well as from Boscan, Cerro Negro, and Prudhoe Bay petroleums.[1,2] The identification of these trace metallo-organic compounds will not only provide an improved understanding of the biogeochemical mechanisms responsible for their presence but also enhance the likelihood of novel removal methods for these severe catalyst poisons during petroleum processing.[3–5]

In this regard, we have developed a novel combination of C-18 reverse-phase and cyano normal-phase HPLC-GFAA analysis to separate and purify the highly polar nickel non-porphyrin constituents present in a Wilmington extract.

Bonded-phase HPLC separations, either reverse phase or cyano columns, offer several unique advantages over the more conventionally used silica columns.[6] Because polar solvents such as methanol and water can be used, bonded-phase packings are capable of separating highly polar metal-containing complexes. These highly polar complexes would be irreversibly bonded to silica because most polar solvents rapidly and seriously degrade silica packings.

Furthermore, reverse-phase packings allow for partition separations in which polar compounds generally elute before non-polar constituents. Conversely, cyano columns can be operated in either normal or reverse-phase modes, thus providing increased flexibility over silica-packed columns. We report studies directed toward the preparative isolation and identification of polar nickel non-porphyrin complexes from Wilmington heavy crude petroleum (49 ppm V, 60 ppm Ni), using element-selective HPLC-GFAA analysis. Details of the HPLC-GFAA and sample preparation procedures have previously been published.[1,2]

Since, unlike porphyrin complexes, non-porphyrin complexes have no discernible characteristic electronic spectra,[7] element-selective detection becomes essential. We have thus chromatographed a variety of vanadium and nickel-containing model compounds in order to compare the molecular properties and retention behavior of the known standards to those of the naturally occurring constituents present in the petroleum extracts.

Finally, we report on results obtained using a variety of off-line mass spectral techniques, including electron impact (EI), field desorption (FD), and fast atom bombardment (FAB), for both the model compounds and nickel non-porphyrins isolated from Wilmington petroleum.

ACCOMPLISHMENTS DURING FY 1984

Thirty grams of Wilmington oil dissolved in 30 mL of p-xylene was contacted with three equal volumes of pyridine/H_2O (4:1) to yield 1 liter of extract. The crude extract was filtered and evaporated to 40 mL (25× concentrated). A mass balance performed using the GFAA, with aqua regia conditions (3:1 HCl:HNO_3 v/v) and standards plots, revealed that 65% of the nickel had been extracted.

Preparative separations were performed using an octadecylsilane (ODS) C-18 Altex HPLC column (10 mm × 25 cm) with a solvent gradient from 100% MeOH to 100% CH_2Cl_2. The highly polar nickel compounds eluted using MeOH, and several 250 μL injections were performed to yield a separate fraction rich in nickel non-porphyrin compounds. A mass balance indicated that 97% of the injected nickel was recovered.

This first fraction, containing nearly 80% of the injected nickel, was observed to have little visible background absorbance (410 nm). In comparison, fraction 2 eluted with CH_2Cl_2 and had much greater visible background absorbance, indicating the presence of metallo-porphyrin complexes.

Since off-line identifications using mass spectrometry require relatively pure fractions, we have concentrated our efforts on fraction 1. This fraction,

*This work was supported by the Assistant Secretary for Fossil Energy, Office of Oil, Gas, and Shale Technology of the U.S. Department of Energy through the Bartlesville Project Office under Contract No. DE-AC03-76SF00098.

†Chevron Research Co., Richmond, CA.

the more polar of the two separated classes of nickel chelates, has no detectable metallo-porphyrins, on the basis of the absorbance at 410 nm, but does show a maximum UV-VIS absorbance at 275 nm.

Purification of the Polar Nickel Non-Porphyrin-Rich Fraction

We have found, through rechromatography of fraction 1 on the ODS column, that the concentration of nickel can be increased from ~8,000 to ~11,000 ppm (Table 1). Although these high metal concentrations approach those generally considered sufficient for mass spectral analysis, higher levels would even further increase the likelihood of identifying these nickel-containing species.

Further purification, therefore, was performed using a cyano Altex (4.5 mm × 25 cm) analytical column with a gradient from 100% CH_2Cl_2 to 100% MeOH. The naturally occurring nickel complexes eluted at 50% to 100% MeOH (Fig. 1) and therefore can be judged to be more polar than our synthesized nickel non-porphyrin standards that elute at approximately 10% MeOH. In contrast, $NiCl_2$ eluted at approximately 28 minutes, which is later than band II (Fig. 1), thus precluding the possibility of inorganic nickel.

A more likely possibility is that these compounds occur predominantly as nickel carboxylic acid salts. Thin-layer chromatography (TLC, Whatnon KSF) analysis has indicated that the nickel compounds shown in Fig. 2 have very similar retention behavior compared to the petroleum-derived com-

Table 1. Nickel concentrations of preparatively collected fractions from Wilmington petroleum submitted to mass spectroscopy analysis.[a]

	ODS I	ODS II[b]	Cyano peak I[c]
ppm Ni	8,040	11,000	14,250
Weight of collected fraction (mg)	60	25.2	4.0
Weight % nickel complexes[d]	4.1	5.7	7.4

[a]Concentrations determined using aqua regia conditions and standards plots.

[b]Rechromatography of ODS I, using ODS column.

[c]Rechromatography of ODS II, using cyano column.

[d]Assumed molecular weight of complexes, 300 daltons.

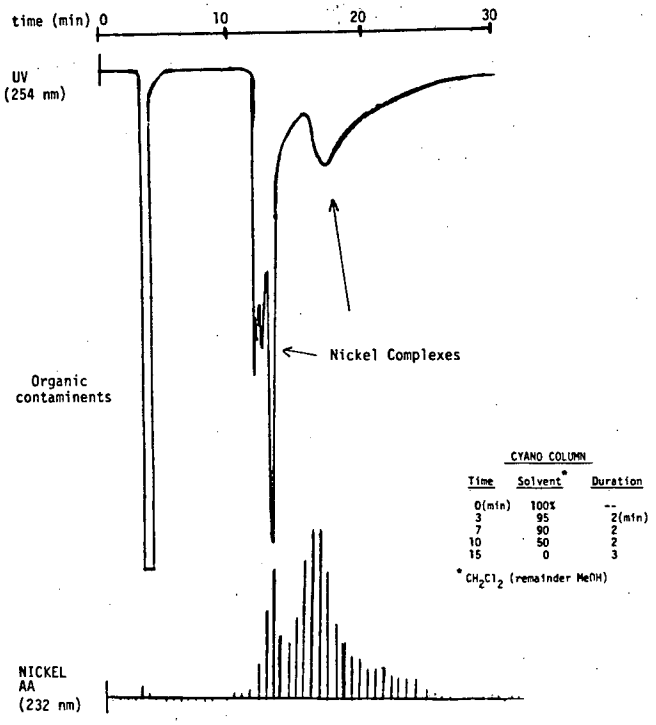

Figure 1. Purification of nickel complexes isolated from Wilmington petroleum using element-selective cyano HPLC-GFAA analysis. (XBL 8411-4661)

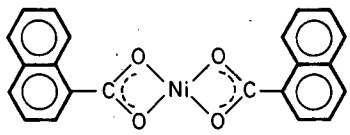

Nickel Napthenate

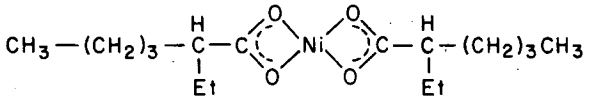

Nickel 2-Ethylhexanoate

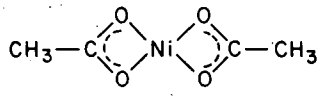

Nickel Acetate

Figure 2. Model nickel carboxylic-acid salt complexes. (XBL 8412-5428)

plexes. We are currently chromatographing these standards, as well as others we are preparing, and will be using the cyano column in conjunction with HPLC-GFAA to more accurately check the retention times of these metal salt complexes.

Mass Spectrometry Analysis

We are currently analyzing our isolated nickel-rich fractions using mass spectrometry (MS). Our most recently submitted sample contained approximately 7.0% of a concentrated nickel fraction (assumed molecular weight = 300 daltons), and we have found a series of compounds (approximate molecular weight = 250) that we are presently analyzing by high-resolution MS for nickel (Fig. 3). We are also analyzing, by fast atom bombardment (FAB) MS and other techniques, the model non-porphyrin complexes (Ref. 2 and Fig. 2) to obtain their characteristic fragmentation patterns. We have found that all of the model "metallo-" compounds from Ref. 2 give nickel-containing parent ions.

Of primary importance is whether the metal complexes extracted from the petroleum will volatilize when MS techniques such as FAB are used. To determine if the isolated nickel non-porphyrin complexes undergo thermal decomposition with MS conditions, we are performing thermal gravimetric analyses (TGA) and subsequently analyzing for nickel content. This analysis has already shown that 98% of the nickel is nonvolatile, so that it will be difficult to analyze these thermally unstable compounds with MS techniques.

Summary

We have developed a technique whereby highly polar nickel non-porphyrin compounds can readily be isolated from heavy crude petroleums. Furthermore, we have compared the electronic spectra, HPLC retention behavior, and mass spectral fragmentation patterns of these compounds to those of synthesized model compounds. On the basis of the resulting information, we have concluded that the isolated complexes are conceivably present as nickel carboxylate salts.

We strongly feel that the eventual identification of these metallo-non-porphyrin complexes, using off-line mass spectroscopy techniques, will facilitate

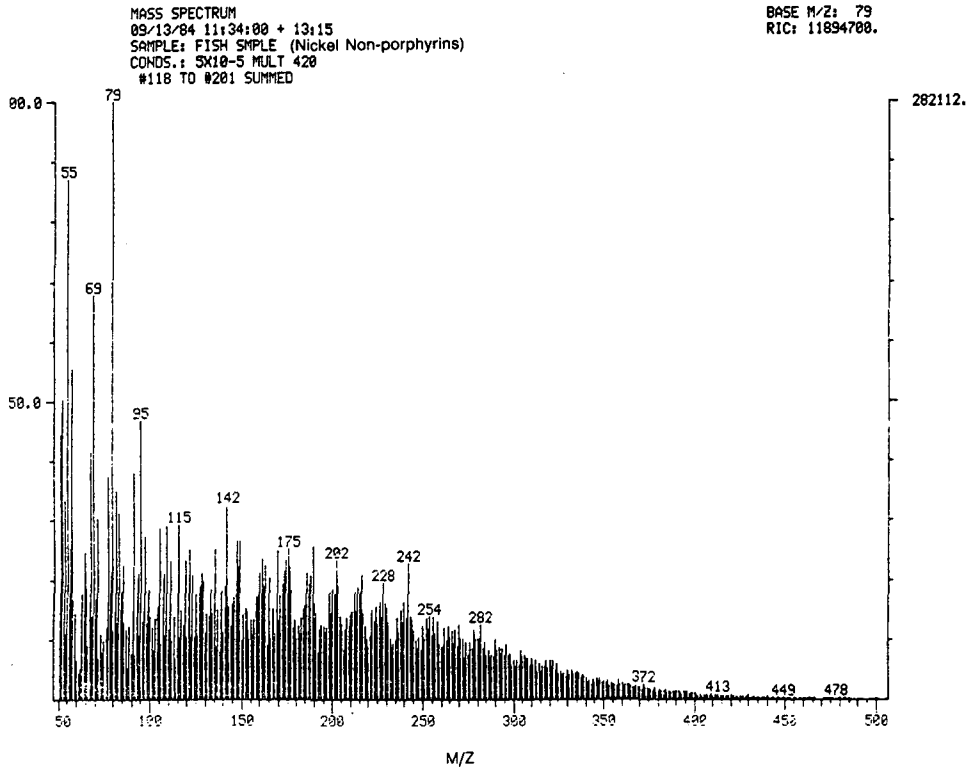

Figure 3. Mass spectroscopy of a homologous series of compounds isolated from Wilmington petroleum. (XBL 8411-4660)

an improved understanding of both the bio-origin and processing aspects of fossil fuel products.

PLANNED ACTIVITIES FOR FY 1985

Efforts will continue to focus on using mass spectroscopy to identify specific classes of metallo-non-porphyrins isolated from petroleums using preparative HPLC.

We also plan to study these identified metal complexes, using polymer-supported ligand exchange reactions, for the purpose of developing novel techniques for removing nickel and vanadium compounds from complex matrices.

REFERENCES

1. Fish, R.H. and Komlenic, J.J. (1984), *Anal. Chem. 56*, p. 510.
2. Fish, R.H. Komlenic, J.J., and Wines, B.K. (1984), *Anal. Chem. 56*, p. 2452.
3. Fish, R.H. and Tannous, R.S. (1982), *Organometallics 1*, p. 1238.
4. Hung, C.W. and Wei, J. (1980), *Ind. Eng. Chem. Process Des. and Dev. 19*, p. 250.
5. West, M. (1984), Ph.D Thesis, University of California, Berkeley.
6. O'Laughlin, J.W. (1984), *J. Liquid Chromatog. 7(5-1)*, p. 127.
7. Spencer, W.A., Galobardes, J.F., Curtis, M.A., and Rogers, L.B. (1982), *Sep. Science Tech. 17*, p. 797.

Polymer Pendant Ligand Chemistry: Reactions of Organoarsonic Acids and Arsenic Acid with Catechol Ligands Bonded to Polystyrene-Divinylbenzene and Regeneration of the Ligand Site by a Simple Hydrolysis Procedure*

R.H. Fish and R.S. Tannous

The use of polymer-supported pendant ligands for metal-ion removal is a well-developed field.[1,2] More recent studies have focused on the selective reactions of these polymer-bonded ligands and include separations of biological substrates,[3] protein fractionation,[4] racemates,[5] and transport of cations through membranes.[6]

Interestingly, very few of the reported selective reactions incorporate a chemical reaction for the metal-ion removal step; rather, they usually entail an ion exchange or binding phenomenon for reaction to occur.[7,8] Additionally, this field has given little attention so far to the important area of processing complex matrices such as synthetic fuels and petroleum crudes for the removal and recovery of metal-compound contaminants.[9]

In this article, we describe a novel method for reactions of organoarsonic acids and arsenic acid, known to be present in oil shale and its pyrolysis products,[10-12] with catechol ligands bonded to either 2% or 20% cross-linked methylated polystyrene-divinylbenzene (PS-DVB) resins.[13]

ACCOMPLISHMENTS DURING FY 1984

The bonded catechol ligands were reacted with phenylarsonic acid, **1**, and methylarsonic acid, **2**, in benzene or with arsenic acid, **3**, in 90% aqueous ethanol to provide the corresponding polymer bonded 1:2, **1** and **2** (Eq. 1) or 1:3, **3**, arsenic catecholates.[14,15]

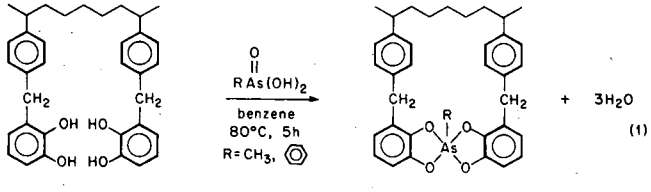

Table 1 provides the concentrations (mmole As/g of resin) of **1–3** removed from solution and compares the 2% cross-linked resin to the 20% analogue. It is evident from the results in Table 1 that high concentrations of compounds **1–3** are removed from solution with both the 2% and 20% cross-linked catechol bonded resins. We verified the 1:2 and 1:3 ratios of arsenic to catechol for **1**, **2**, and **3**, respec-

*This work was supported by the Assistant Secretary for Fossil Energy, Office of Oil, Gas, and Shale Technology of the U.S. Department of Energy through the Bartlesville Project Office under Contract No. DE-AC03-76SF00098.

Table 1. Concentration of arsenic compounds **1–3**, removed from solution using both 2% and 20% cross-linked, catechol-bonded PS-DVB resins.[a]

Arsenic compound	2%[b,c] Conc. (mmole As/g)	% Removed	20%[b,c] Conc. (mmole As/g)	% Removed
1	0.503[d]	100	0.232	86
2	0.307	62	0.20	74
3	0.212	64	0.124	69

[a]100 mg of catechol-bonded resin, 2% or 20% cross-linked, containing 1.0 mmole/g, 11% by weight of catechol or 0.538 mmole/g, 5.92% by weight of catechol, respectively.

[b]Reaction conditions for compounds **1** and **2**: initial arsenic to catechol concentration is 1:2 at 80°C for 18 hours in benzene (10 mL) under nitrogen.

[c]Reaction conditions for compound **3**: initial arsenic to catechol concentration is 1:3, 81°C, 17 hours, 90% ethanol (10 mL) under nitrogen.

[d]After reaction, the beads were filtered and washed well with hot methanol, quartz water, and again with methanol. The washings were added to the filtered solution and analyzed for arsenic by single-cup graphite furnace absorption spectrometry.

tively, by varying the ratio of the two reactants and finding the maximum concentrations removed at the above-mentioned stoichiometries.

In addition, we attempted to verify structures of the polymer-bonded arsenic catecholates by comparing the infrared spectrum (KBr) of the polymer-supported catechol resin with those resins containing compounds **1–3** after reaction with the bonded catechol ligands. Unfortunately, infrared bands due to As-O stretching frequencies, ~680–700 cm^{-1}, were masked by PS-DVB aromatic C-H deformations as well as by those of the catechol ligands. However, we did see dramatic changes in the IR spectra of the bonded arsenic catecholates. For example, IR bands at 1250, 1115, and 870 cm^{-1}, attributed to the OH deformations of the bonded catechol ligands, disappeared in the IR spectra of the bonded arsenic catecholates. We feel that this result substantiates reactions of **1**, **2**, and **3** with the bonded catechols to provide the biscatecholates (Eq. 1) and the tricatecholate for **3**.

The equilibrium values of removal from solution of compounds **1–3** were ascertained by plotting mmoles of arsenic per gram of resin (20%) versus time (Fig. 1). From the results in Fig. 1, compound removal values at equilibrium are **1** > **2** > **3** for the 20% cross-linked resin, and the initial rate ratio for **1**/**2** is ~7.3. This initial rate ratio for **1** and **2** could not be readily compared to **3** because of solvent

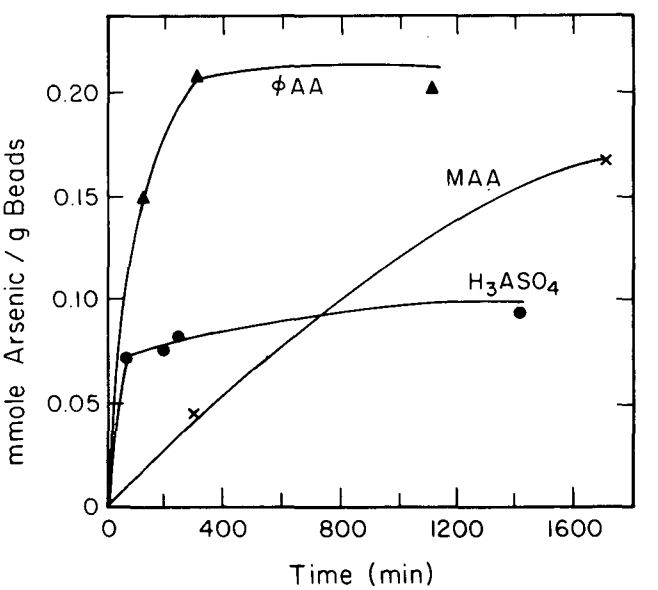

Figure 1. Removal of ΦAA (**1**), MAA (**2**), and H_3AsO_4 (**3**), from solution with 20% cross-linked catechol-bonded resin (5.92% catechol by weight). (XBL 8412-5429)

differences in their respective reactions, i.e., benzene for **1** and **2** and aqueous ethanol for **3**.

It is also apparent from Table 1 that the 2% cross-linked swellable resins contain the higher concentration of catechol and consequently can remove almost twice the concentration of arsenic compounds **1–3** from solution. However, for this application, we found the macroreticular 20% cross-linked resins easier to handle in filtrations and constant reuse; thus we preferred to use these resins in both removal and regeneration experiments.

In this regard, the ligand site could easily be regenerated by a simple hydrolysis procedure using a solution of sodium carbonate (6.3×10^{-2} *M*) in either 63% aqueous ethanol or quartz-distilled water at 65°C for 1 hour. Figure 2 demonstrates the rapid ligand regeneration reaction for the 20% cross-linked resins containing the arsenic catecholates. Importantly, from 40% to 85% of the arsenic compounds **1–3** are recovered after approximately the first 10 minutes of hydrolysis, with rates of hydrolysis being **2** > **1** > **3**. Further arsenic compound hydrolysis is provided after 1 hour (5–10%) by reaction with a sodium bicarbonate solution (7×10^{-2} *M*, 1 hour, 65°C), and this also regenerates the catechol site for reuse. It is then important for continued reuse to wash the catechol-bonded resins with hot water and methanol to remove carbonates and finally dry the resin under vacuum (95°C, 1 hour) to remove water. The above-mentioned removal (uptake) and hydrolysis procedures were repeated at least three times for compounds **1–3** with consistent results (Table 1).

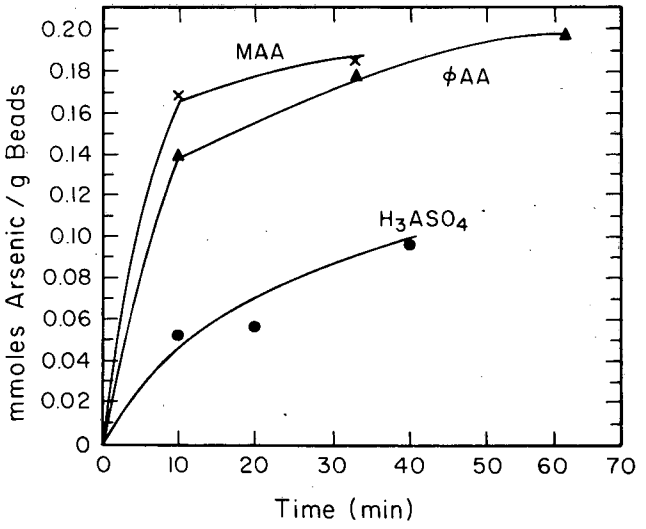

Figure 2. Hydrolysis (Na_2CO_3, 1 hour, 63% aqueous ethanol) of ΦAA (**1**), MAA (**2**), H_3AsO_4 (**3**), bonded catecholates (20% cross-linked resin). Initial arsenic concentration on the resin for **1** was 0.232 mmoles As/g; for **2**, 0.2 mmoles As/g; and for **3**, 0.124 mmoles As/g.

(XBL 8412-5430)

PLANNED ACTIVITIES FOR FY 1985

Clearly, these polymer-pendant ligand reactions with organometallic and inorganic compounds have the potential of being highly selective, as with the arsenic compounds discussed, especially in nonpolar solvents where solubility dictates reactivity. We are continuing our studies of polymer-pendant ligand chemistry directed toward removal of metal compounds from synthetic fuels and petroleums, using appropriate compounds found in the above-mentioned complex matrices as well as other bonded ligands.

REFERENCES

1. For the synthesis and properties of cross-linked polymers, see Frechet, J.M. and Farrall, M.J. (1977), in *Chemistry and Properties of Cross-Linked Polymers,* S.S. Labana, Ed., Academic Press, New York.
2. Blasius, E. and Brazio, B. (1967), in *Chelating Ion Exchange Resins in Chelates in Analytical Chemistry*, H.A. Flaschka and J.A. Barnard, Eds., Marcel Dekker, New York.
3. Cram, D.J. and Cram, J.M. (1978), *Acc. Chem. Res. 11*, p. 8.
4. Porth, J., Carlson, J., Olsson, I., and Belfrage, G. (1975), *Nature 258*, p. 598.
5. Davankov, V.A., Rogozhin, S.V., Semechkin, A.V., and Sachkova, T.P. (1973), *J. Chromatog. 82*, p. 359.
6. Kobuke, Y., *et al.* (1976), *J. Am. Chem. Soc. 98*, p. 7414.
7. Warshawsky, A., *et al.* (1979), *J. Am Chem. Soc. 101*, p. 4249 and references therein.
8. Drago, R.S., Gaul, J., Zombeck, A., and Straub, D.K. (1980), *J. Am. Chem. Soc., 102*, p. 1033 and references therein.
9. Flett, D.S. and Pearson, D. (1975), *Chem. and Ind.* p. 639.
10. Fish, R.H., *et al.*, (1983), *J.C.S. Chem. Commun.* p. 490.
11. Fish, R.H. (1983), "Geochemistry and Chemistry of Oil Shales," F.P. Miknis and J.F. Mckay, Eds., ACS Symposium Series 230, p. 423.
12. Brinckman, F.E., Weiss, C.S., and Fish, R.H. (1983), in *Chemical and Geochemical Aspects of Fossil Energy Extraction*, Chap. 13, T.F. Yen, F.K. Kawahara, R. Hertzberg, Eds., Ann Arbor Science, Ann Arbor, MI.

13. Synthesized by reaction of catechol with 2% or 20% chloromethylated polystyrenedivinylbenzene resins in the presence of stannic chloride to provide an 11% by weight (2%) and 6% by weight (20%) incorporation of catechol in the polymer. See Warshawsky, A. and Kahana, N. (1981), *J. Am. Chem. Soc. 104,* p. 2663 and Iwabuchi, S., *et al.* (1981), *J. Polym. Sci. 19,* p. 785 for similar synthetic routes to bonded catechol.

14. Fish R.H. and Tannous, R.S. (1982), *Organometallics 1,* p. 1238.

15. Fish, R.H. and Tannous, R.S. (1984), manuscript submitted for publication to *Organometallics.*

Homogeneous Catalytic Hydrogenation: Regioselective Reduction of Polynuclear Heteroaromatic Compounds Catalyzed by $(PPh_3)_3RuHCl$*

R.H. Fish, J.L. Tan, and A.D. Thormodsen

We have recently reported on the regioselective hydrogenation of polynuclear heteroaromatic compounds using a variety of transition metal complexes.[1-3] The types of aromatic substrates we have investigated contain a single nitrogen or sulfur heteroatom in a two or three fused ring aromatic structure (compounds **1-7**, Fig. 1) and are intended to model the types of compounds known to be in coal-derived liquids and shale oil. It is hoped that a better understanding of these reductions will lead to improvement of the existing processes using hydrogen gas for refining and upgrading coal and other synthetic fuels.

In our earlier studies,[1-3] we found that ruthenium[1,2] and rhodium[3] complexes show the most activity toward selective reduction of the heteroaromatic ring in the types of substrates therein described when compared with the Fe, Mn, and Co complexes previously investigated.[1,2] We have now discovered that hydridochlorotris-(triphenylphosphine) ruthenium (II) $[(PPh_3)_3RuHCl]$ and hydrogen gas, with the heterocycle acting as base, is an exceptionally active catalyst for the types of reactions described. Interestingly, it is more active by a factor of 3 than its rhodium analogue $(PPh_3)_3RhH_2Cl$, which we have studied earlier.[3] This ruthenium complex is a well-known hydrogenation catalyst and has been used to reduce a variety of compounds, including olefins, aldehydes, ketones, and nitro compounds.[4-8] To our knowledge, this is the first reported use of this catalyst in the selective reduction of polynuclear heteroaromatic compounds.

In this article, we report on the regioselective reductions of compounds **1-7** with regard to the relative rate of hydrogenation of the substrates both individually and in a mixture with other substrates and model coal compounds. We will also present

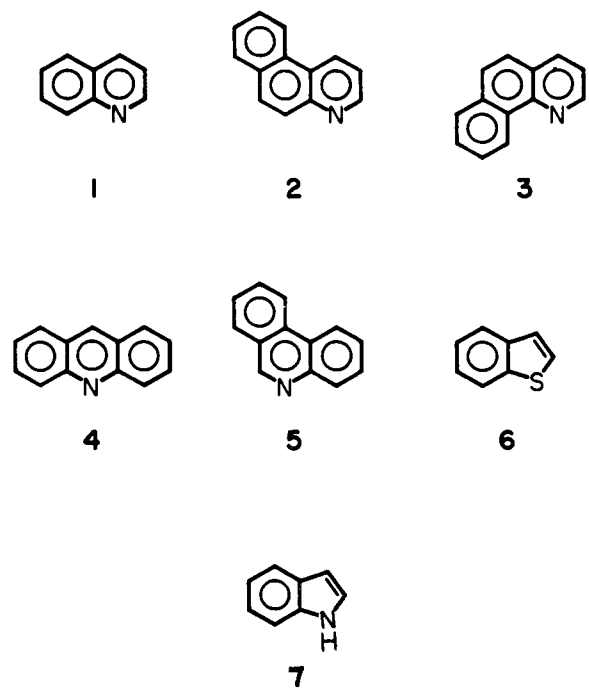

Figure 1. Polynuclear heteroaromatic substrates reduced in hydrogenation reactions catalyzed by $(PPH_3)_3RuHCl$: **1**, quinoline; **2**, 5,6-benzoquinoline; **3**, 7,8-benzoquinoline; **4**, acridine; **5**, phenanthridine; **6**, benzothiophene; and **7**, indole. (XBL 8412-5434)

*This work was jointly funded by the Director, Office of Energy Research, Office of Basic Energy Sciences, Chemical Sciences Division, and the Assistant Secretary for Fossil Energy, Office of Coal Liquefaction Technology of the U.S. Department of Energy, through the Pittsburgh Energy Technology Center under Contract No. DE-AC03-76SF00098.

data on the reduction of one of these compounds, **1**, using deuterium gas in place of hydrogen gas. As well, we will establish the binding of **8** to the ruthenium hydride complex by nuclear magnetic resonance (NMR) spectroscopy. We will then propose a reduction scheme that accounts for our observed results.

ACCOMPLISHMENTS DURING FY 1984

Regioselective Hydrogenation

Table 1 contains the initial and relative rates for the selective reduction of the heterocyclic ring in compounds **1–7** (N-ring compounds **1–5, 7**; S-ring compound **6**) catalyzed by $(PPh_3)_3RuHCl$ under a standard set of conditions. The catalyst was generated *in situ* from $(PPh_3)_3RuCl_2$ and hydrogen gas and our substrates, which were basic enough to neutralize the HCl formed during this reaction. The substrate-to-catalyst ratio was 10:1 in all cases, with initial turnover numbers (per Ru per hour) varying from more than 66 to 0.08. The order of individual reduction rates was **5** > **4** >> **1** > **7** > **2** > **6** > **3**, reflecting both steric and electronic effects. For the reduction of **1** and its two benzoderivatives, **2** and **3**, steric effects are clearly important. Compound **3**, the most sterically hindered at the nitrogen, is reduced at the slowest rate, while compound **1**, with the least hindrance, is reduced the fastest. However, a comparison of the reduction rates of **6** and **7** shows that other effects are in operation. Since these two molecules differ only in the identity of the heteroatom, the rate differences cannot be sterically caused. Electronic effects are most likely to be the cause of the differing rates, either because of the complexing ability of the heteroatom or because of the electron density on the adjacent double bond.

Table 1. Rates of reduction of compounds **1–7** under hydrogenation conditions using $(PPh_3)_3RuHCl$ as catalyst.[a]

Compound	Product[b]	Rate (%/min)[c]	Relative rate[d]
1	1,2,3,4-Tetrahydroquinoline	0.47	1.00
2	1,2,3,4-Tetrahydro-5,6-benzoquinoline	0.059	0.12
3	1,2,3,4-Tetrahydro-7,8-benzoquinoline	0.014	0.03
4	9,10-Dihydroacridine	4.3	9.2
5	9,10-Dihydrophenanthridine[e]	> 11	> 24
6	2,3-Dihydrobenzothiophene	0.041	0.09
7	2,3-Dihydroindole	0.085	0.18

[a]Conditions: 1 mmole of substrate (compounds **1–7**), 0.1 mmole of $(PPh_3)_3RuCl_2$, 310 psi H_2 (initial), 20 mL benzene as solvent, temperature = 85°C (± 0.5°C). The active catalyst, $(PPh_3)_3RuHCl$, is formed *in situ* from $(PPh_3)_3RuCl_2$ and hydrogen, with the substrate acting as base. Figure 1 shows the structure of the substrate compounds.

[b]Analysis by capillary gas chromatography.

[c]Pseudo-zero order rate, followed to approximately 50% conversion.

[d]Rates are relative to quinoline; i.e., each reduction rate was divided by the rate for quinoline (0.47) to obtain the values given.

[e]Phenanthridine was reduced too rapidly to determine a rate using our technique. Reduction was complete within 9 minutes, so the value given for this rate is a lower bound.

Inhibition Studies

Since the rate differences given in Table 1 seem partly to reflect steric and electronic requirements in the binding of compounds **1–7** to the ruthenium metal center, experiments were carried out in which **1** was reduced in the presence of an equimolar amount of another compound that could potentially compete with **1** for binding to the ruthenium. Table 2 clearly shows that the reduction of **1** was inhibited by compounds **2, 7, 8, 9, 10**, and **11**, but was unaffected by **3** and **6**. There were no enhancements in rate such as we have observed with the rhodium analogue.[3] The effects of compounds **3** (7,8-benzoquinoline) and **9** (2-methylpyridine), when compared to the effect of **2** (5,6-benzoquinoline) and

Table 2. Relative rates of reduction of **1** in the presence of other compounds.[a]

Added compound	Relative rate[b]
None	1.0
2[c] 5,6-Benzoquinoline	0.79
3[c] 7,8-Benzoquinoline	0.98
6[c] Benzothiophene	1.0
7[c] Indole	0.66
8 1,2,3,4-Tetrahydroquinoline	0.34
9 2-Methylpyridine	0.85
10 3-Methylpyridine	0.00
11 Carbazole	0.89

[a]Conditions: 1 mmole of **1**, 1 mmole of added compound, 0.1 mmole of $(PPh_3)_3RuCl_2$, 310 psi H_2 (initial), 20 mL benzene as solvent, temperature = 85°C (± 0.5°C).

[b]Rates are relative to rate of reduction of **1** alone (0.47, see Table 1).

[c]In these cases, the added substrate was reduced along with **1**; see Table 3 and discussion.

10 (3-methylpyridine), provide insight into the steric requirements for binding to the ruthenium. Compounds **2** and **10** should have less hindrance at the nitrogen than the corresponding isomers **3** and **9**. In both cases, the less sterically hindered **2** and **10** show greater inhibition, indicative of more effective competition with **1** for catalyst metal centers than shown by **3** and **9**. Compounds **6** (benzothiophene) and **11** (carbazole) indicate the importance of basicity in determining strength of binding, since both of these molecules are less basic than **1**, suggesting that they should not compete with it for catalyst. Both these compounds show little or no affect on the reduction rate of **1**, consistent with the assumption that they do not competitively bind. Compound **8** (1,2,3,4-tetrahydroquinoline) is the product of reduction of **1** and strongly inhibits its reduction by a factor of 0.34. This indicates that product inhibition may be an important factor in many of these reductions, in which the products are often stronger bases than the reactants. Finally, compounds **2, 3, 6**, and **7** were reduced along with **1**, providing additional insight into binding effects and rates.

Binding and Selectivity in Competitive Reductions

Table 3 contains data derived from the experiments described in the previous two sections. The first column of rates was derived by dividing the individual reduction rate of **1** by the individual reduction rates of **2, 3, 6**, and **7**, respectively (data taken from Table 1), to provide a ratio representing the rate of reduction of **1** relative to each other compound. The second column of rates was calculated in the same manner, except that the rate data used are for the competitive reduction of **1** in the presence of an equimolar amount of **2, 3, 6**, and **7**, respectively. In all four cases, the relative rate for the reduction of **1** versus the other compounds is greater in the mixture, indicating a selectivity toward the reduction of **1**. The most dramatic example is for compound **6** (benzothiophene). Compound **1** is reduced 11.5 times faster than **6** when the reductions are carried out separately, but is reduced 43 times faster than **6** when the reduction is carried out in a mixture of the two. In the second case, the more basic **1** can compete for catalyst more effectively than **6**, resulting in a higher relative rate.

Table 3. Selectivity for the reduction of **1** in competition with other reducible substrates.

Compound	Relative rate in separate reductions[a]	Relative rate in mixture[b]
2	8.0	11
3	33.6	42
6	11.5	43
7	5.5	8.2

[a]Values derived from data in Table 1 (separate reductions) by dividing the initial rate of reduction of **1** by the initial rate of reduction of the other compound.

[b]Conditions: 1 mmole of **1**, 1 mmole of added compound, 0.1 mmole of $(PPh_3)_3RuCl_2$, 310 psi H_2 (initial), 20 mL benzene as solvent, temperature = 85°C (±0.5°C). Figures obtained by dividing the initial rate of reduction of **1** by the initial rate of reduction of added compound.

Deuterium Gas Experiments

In previous studies,[3,9,10] the substitution of deuterium gas for hydrogen gas in catalytic reductions has been found to provide useful mechanistic information. Compound **1** was reduced for 72 hours at 85°C in a 10:1 substrate-to-catalyst ratio, yielding 100% deuterated 1,2,3,4-tetrahydroquinoline. Analysis of this product by 200 MHz ^1H NMR provides the results depicted in Eq. (1):

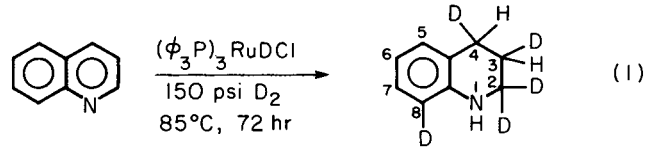

(1)

The product had 1.8 deuteriums at position 2, one deuterium each at positions 3 and 4, and 0.8 deuterium at position 8. The nitrogen was not observed to be deuterated because of the rapid exchange of this position with traces of water during workup.

When this same reduction was carried out for 150 minutes, to approximately 50% conversion, the deuterium substitution pattern was much the same as in the case of complete reduction. Position 2 was substituted with 1.85 deuteriums, positions 3 and 4 had one deuterium each, and 0.2 deuterium was found at position 8. The unreduced quinoline was also observed in the NMR spectrum and showed 0.5 deuterium substitutions at position 2.

Finally, compound **8** (1,2,3,4-tetrahydroquinoline) was reacted with deuterium and the ruthenium catalyst under the same conditions used to reduce **1**. After 4.5 hours, the reaction product

was analyzed by 200 MHz ^{1}H NMR to give the results in Eq. (2):

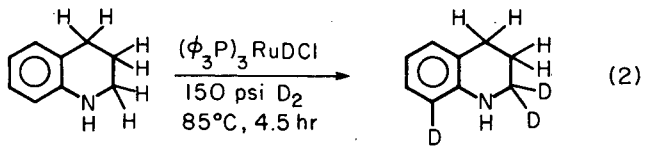

(2)

12

Position 2 was substituted with 1.8 deuteriums, and position 8 with 0.1 deuterium. A mass spectrum was also obtained for this compound, giving m/e = 135 for the base (M-1) peak, and indicated d_1, d_2 and d_3 products.

Reduction Mechanism

The deuterium exchange reported above can be accounted for by several plausible intermediates, incorporated together in our proposed reduction scheme (Fig. 2).

The overall reduction occurs in the order **1** ⇄ **A** ⇄ **B** → / **C** / **A**. The first step, **1** ⇄ **A**, is the necessary prior coordination of **1** to the ruthenium metal catalyst. At this stage, as we have shown in our competitive rate results, coordination can be inhibited by competition from another coordinating substrate, slowing the overall rate of hydrogenation.

After coordination, the reversible reduction of the C-N double bond occurs (step **A** ⇄ **B**). It is the reversibility of this step that accounts for the incorporation of deuterium into position 2 of the unreduced quinoline. It accounts as well for some of the exchange at position 2 of the product, but not all of it. When the reduction was carried out to partial completion, the unreduced **1** was substituted with 0.5 D at position 2, while the product was substituted with 1.85 D. If all the exchange had occurred through this reversible step, no more than 1.5 D would have been found at position 2 of the product.

The next and final step in the reduction (**B** → **C**) is the irreversible reduction of the 3-4 double bond. This step is shown as irreversible, since only one deuterium was found at the 3 and 4 positions on the product, and also because no **1** was ever observed being formed from **8** by dehydrogenation, under reducing conditions. However, our techniques are not sufficient to rule out a small amount of reversibility. We have found that $(PPh_3)_3RuCl_2$ will catalyze the dehydrogenation of **8** to **1** under nitrogen in refluxing benzene, suggesting the possibility of a fully reversible pathway from **1** to **8** and back again. We do not know if the reduction is inter- or intramolecular. It may proceed by an intramolecular addition of hydrogen from the nitrogen-bound ruthenium, or, more likely, it may occur by coordination of a ruthenium to the 3-4 double bond, as with an olefin.

In order to provide more information about the complex **C**, a 1:1 mixture of **8** and preformed $(PPh_3)_3RuHCl$ was prepared in an NMR tube, and its 200 MHz ^{1}H NMR spectrum taken. All of the

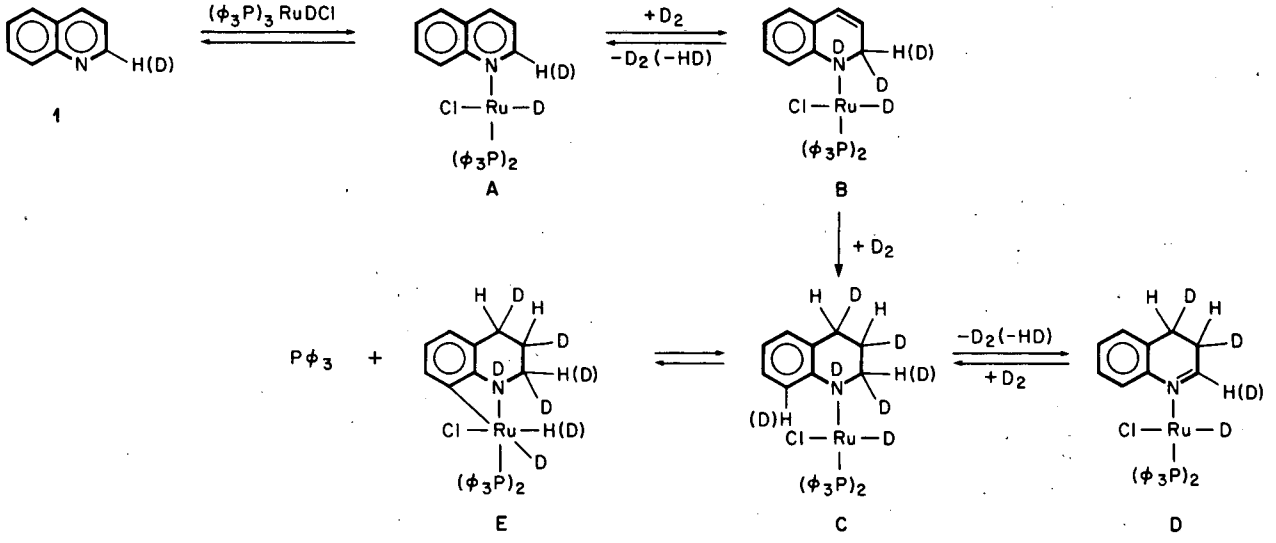

Figure 2. Proposed scheme for reduction of compound **1** (quinoline) when catalyzed by $(PPH_3)_3RuHCl$.
(XBL 8412-5435)

signals for **8** were found, and were shifted from the signals of the free compound, with the relative areas of the peaks remaining the same. Thus binding to the metal center had occurred. The largest shift (2.4 ppm) occurred at the **1** position, consistent with coordination to the nitrogen. The other shifts were 0.2 ppm (H-2) and 0.25 ppm (H-8), consistent with the close proximity of these positions to the nitrogen binding site.

To account for the exchange of deuterium found when starting with **8**, the imine intermediate **D** is proposed. It is known that $(PPh_3)_3RuCl_2$ is an active catalyst for alkyl amine chain scrambling and deuterium exchange at carbons adjacent to nitrogen in amines.[9,11,12] This type of reactivity is generally explained by proposing hydridochlororuthenium-imine complexes formed by dehydrogenation of amines. Such an imine intermediate has in fact been observed by Jung *et al.*[9] We are proposing that the reversible formation and reduction of the imine intermediate **D** accounts for the exchange of deuterium found on **8**, as well as part of the exchange found on the product when reducing **1**. Such an intermediate and the imine itself would be unstable to both oxidation and reduction as well as being present in only small quantities. This would explain why we have failed to observe any free imine in these reactions.

Instead of a reversible dehydrogenation/ hydrogenation mechanism, the exchange may occur through the formation and hydrogenolysis of a metal-carbon bond at the 2 position. If the metal-nitrogen bond remains intact, this intermediate would be a metala-azacyclopropane (not shown in Fig. 2 scheme). Such compounds have been reported by Crawford *et al.*[13,14] and have been postulated by Laine *et al.*[10] to explain their results with deuterium exchange reactions on tertiary alkyl amines catalyzed by rhodium clusters.

One final result to be explained is the exchange of the aromatic C-H bond at the 8 position. A means for this exchange to occur is through the formation and cleavage of a four-membered cyclometallated ring, intermediate **E**. This complex is similar to five-membered rings formed from **3** and osmium and ruthenium clusters by Bruce *et al.*[15,16] Loss of triphenylphosphine must occur as indicated to provide an 18-electron species after oxidative addition to the C-H bond.

The mechanism we have proposed here is somewhat similar to the hydrogenation mechanism previously proposed for $(PPh_3)_3RhCl$.[3] Both these catalysts show the exchange behavior indicated in steps **1**, **A**, **B**, **C**, and **E**. However, only the ruthenium catalyst will exchange deuterium at the "2" position of **8**, as accounted for by intermediate **D**. This is consistent with the fact that the ruthenium catalyst is known to show special reactivity toward amines, as described, while the rhodium catalyst does not.

Conclusions

The complexity of the mechanism of hydrogenation of polynuclear heteroaromatics using $(PPh_3)_3RuHCl$ is apparent from our results; nevertheless, several plausible reduction pathways for **1** may be inferred. The reduction must incorporate an initial reversible step (**A** $\rightleftarrows$ **B**) as well as a post-reduction reversible step (**C** $\rightleftarrows$ **D**) to account for the exchange of deuterium found at the 2 position of both reactant and product. The existence of intermediate **C** is indicated by NMR data, and imine intermediates such as **D** have been reported in similar systems.[9] The irreversibility of the reduction of the 3-4 double bond (**B** $\rightarrow$ **C**) is indicated by the presence of only one deuterium at each carbon but could not be absolutely established. Cyclometallated intermediate **E** is proposed to explain the deuterium incorporation at position 8, while cyclometallated intermediates may also play a role in exchange at the 2 position.

The hydrogenation rates of the various substrates investigated depend on a variety of factors, some of which have been elucidated from competitive hydrogenation experiments. The ability of a substrate to bind to the catalyst, as determined by steric and electronic factors, is of clear importance to the overall rate of reduction. This type of information is valuable when trying to predict the reactivity of chemically complex coal liquids and shale oils.

PLANNED ACTIVITIES FOR FY 1985

We plan to concentrate on the removal of nitrogen (hydrodenitrogenation) from the saturated nitrogen-ring model coal compounds, using homogeneous and bulk metal catalysts.

REFERENCES

1. Fish, R.H., Thormodsen, A.D., and Cremer, G.A. (1982), *J. Am. Chem. Soc. 104*, p. 5234.
2. Fish, R.H. (1983), *Ann. N.Y. Acad. Sci. 415*,, p. 292.
3. Fish, R.H., Tan, J.L., and Thormodsen, A.D. (1984), *J. Org. Chem. 49*, p. 4500.
4. Hallman, P.S., Evans, D., Osborn, J.A., and Wilkinson, G. (1967), *Chem. Comm. 7*, p. 305.

5. Sanchez-Delgado, R.A. and DeOchoa, O.L. (1979), *J. Mol. Catal. 6*, p. 303.
6. Sanchez-Delgado, R.A., *et al.* (1981), *J. Organomet. Chem. 209*, p. 77.
7. Sanchez-Delgado, R.A. and DeOchoa, O.L. (1980), *J. Organomet. Chem. 202*, p. 427.
8. Knifton, J.F. (1975), *J. Org. Chem. 40*, p. 519.
9. Jung, C.W., Fellman, J.D., and Garrou P.E. (1983), *Organometallics 2*, p. 1042.
10. Laine, R.M., Thomas, D.W., Carey, L.W., and Buttril, S.E. (1975), *J. Am. Chem. Soc. 100*, p. 6527.
11. Arcelli, A., Khai, B.T., and Porzi, G. (1982), *J. Organomet. Chem. 231*, p. C31.
12. Khai, B.T., Concilio, C., and Porzi, G. (1981), *J. Org. Chem. 46*, p. 1759.
13. Crawford, S.S. and Kaesz, H.D. (1977), *Inorg. Chem. 16*, p. 3193.
14. Crawford, S.S., Knobler, C.B. and Kaesz, H.D. (1977), *Inorg. Chem. 16*, p. 3201.
15. Bennett, R.L., *et al.* (1972), *J. Chem. Soc. Dalton Trans.*, p. 1778.
16. Bruce, M.I., Goddal, B.L., and Stone F.G.A. (1973), *J. Organomet. Chem. 60*, p. 343.

Reactions of Polynuclear Nitrogen Heteroaromatic Model Coal Compounds with Triruthenium Dodecacarbonyl*

R.H. Fish, A.D. Thormodsen, and T.J. Kim

In order to determine how model coal compounds containing nitrogen heteroaromatic rings react with metal cluster compounds for the purpose of binding and eventually to gain insight into the removal of nitrogen from these compounds, we studied the reactions of quinoline, 1,2,3,4-tetrahydroquinoline, phenanthridine, and dihydrophenanthridine with triruthenium dodecacarbonyl.

These latter polynuclear heteroaromatic nitrogen compounds represent both the unsaturated and saturated analogues, i.e., quinoline and 1,2,3,4-tetrahydroquinoline, which would be present under coal liquefaction conditions in the presence of hydrogen gas.

ACCOMPLISHMENTS DURING FY 1984

The reactions we reported were all run in Schlenk tubes at molar ratios of 1:1, such that we could isolate the products by using several chromatographic procedures and identify their structures by various spectroscopic techniques.

Reaction of Quinoline with $Ru_3(CO)_{12}$

The first polynuclear heteroaromatic nitrogen compound, quinoline, reacted with triruthenium dodecacarbonyl [$Ru_3(CO)_{12}$] to provide a product, **1**, that we unequivocally identified via 200 MHz ^1H nuclear magnetic resonance spectroscopy, mass spectroscopy, and elemental analysis [Eq. (1)].

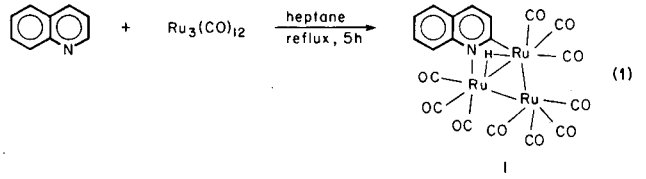

(1)

1

The isolation and structural characterization of compound **1** clearly indicates bonding of the metal cluster to both nitrogen and carbon in the 1,2 position. This exciting result demonstrates that this type of bonding could be utilized to eventually cleave carbon-nitrogen bonds.

The reaction of the saturated nitrogen ring analogue of quinoline, 1,2,3,4-tetrahydroquinoline, provided an interesting product that we tentatively identified via spectroscopic analysis as compound **2** [Eq. (2)].

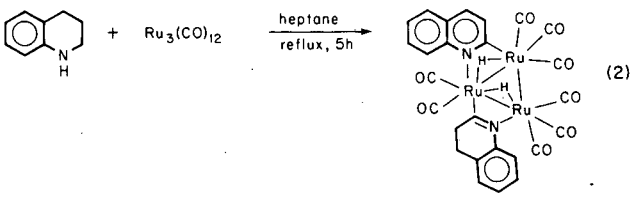

(2)

2

Compound **2** is a dimer; however, we find one nitrogen ring is unsaturated, while the other nitrogen ring is a dihydro derivative. Thus, under the reac-

*This work was supported by the LBL Director's Development Fund through the Department of Energy under Contract No. DE-AC03-76SF00098.

tion conditions, the saturated nitrogen ring is dehydrogenated via mechanisms that need to be elucidated.

Interestingly, when we reacted phenanthridine or dihydrophenanthridine with $Ru_3(CO)_{12}$, we obtained the same compound from either starting material [Eq. (3)].

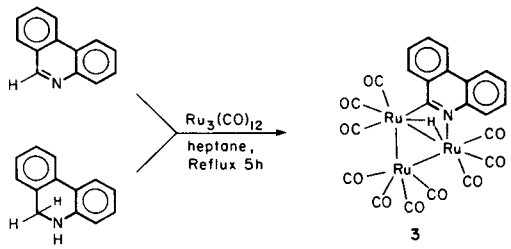

(3)

PLANNED ACTIVITIES FOR FY 1985

We plan to study the reaction of the isolated and identified compounds **1–3** with hydrogen and deuterium gas to determine carbon- and nitrogen-to-ruthenium bond cleavage reactions. We also want to react the polynuclear heteroaromatic nitrogen compounds mentioned above with mononuclear transition metal compounds to ascertain if the metal will bond to both carbon and nitrogen to produce a metalla-azacyclopropane compound, **4**,[1] shown below:

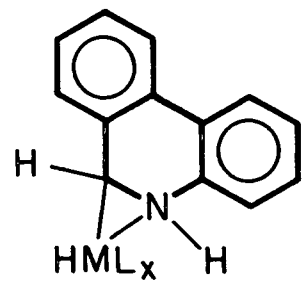

4

This latter compound may be a potential precursor to carbon-nitrogen bond cleavage studies.

REFERENCE

1. Fish, R.H., Thormodsen, A.D., and Kim, T.J. (1985), submitted to *Organometallics* for publication.

Processing of Condensate Waters from Coal Gasification*

C.J. King, J.J. Senetar, P.D. Mackenzie, T.M. Grant, L.J. Poolé, and R.E. Thompson

Large volumes of condensate water are formed when reactor effluents from coal gasification are cooled. Water streams from lower-temperature gasification processes contain large concentrations of ammonia, acid gases, and dissolved organics—notably, phenolic compounds. For both economic and environmental reasons, it is necessary to process these waters sufficiently to allow recycling, probably as make-up to a cooling-tower system.

The principal objective of this project is to provide basic understanding that will enable the development of improved physicochemical processing methods for these condensate waters. Particular attention so far has been given to solvent-extraction and stripping processes and to determining the chemical make-up of real water samples in order that process research may be carried out on a more knowledgeable basis. A new portion of the research concerns the mechanism and kinetics of formation of hydantoin compounds; these compounds have been found in condensate waters and tend to concentrate in cooling-tower blowdowns when processed water is recycled. Hydantoins form upon aging, and the extent to which they are present in fresh condensate water probably depends upon residence time, composition, and temperature of the water in the quench-water circuit of a gasifier.

Earlier research, summarized in the Annual Reports for FY 1979 through FY 1983, has focused upon: (1) determination of individual components contributing to the measured chemical oxygen demand (COD); (2) extraction with both conventional and novel chemically associating solvents, which enable effective removal of COD with the promise of low-energy consumption; (3) interpretation of rates of stripping of ammonia and acid gases from real condensate waters; and (4) combining extraction of ammonia with stripping of acid gases in an innovative process that can recover ammonia as an isolated product.

*This work was supported by the Morgantown Energy Technology Center, Morgantown, West Virginia, through the Assistant Secretary for Fossil Energy, Office of Surface Coal Gasification, Advanced Process Research Program of the U.S. Department of Energy under Contract No. DE-AC03-76SF00098.

ACCOMPLISHMENTS DURING FY 1984

Analysis of Condensate Waters

Several new techniques have been employed in an effort to characterize the remaining unknown COD in previously analyzed condensate water from the Morgantown Energy Technology Center's gasifier run 101; this unknown COD is about 13% of the total. The new techniques include (1) pH-gradient elution; (2) evaporation to a concentrate, followed by contacting with methylene chloride and removal of residual water with a desiccant; (3) various analysis techniques specific for amino acids; and (4) evaporation to dryness, followed by fractional dissolution of the residue in acetone.

For pH-gradient techniques, the solutes in a water sample are first taken up onto a polymeric resin. (Of the resins tested, Rohm & Haas Amberlite XAD-4 has given the best results.) For elution starting at low pH and going to successively higher pH values, the bulk of the unidentified organic nitrogen and organic sulfur have been found in the first (pH = 3) fraction. This suggests that both classes of compounds may be ionized at low pH. Similarly, the largest portion of the unidentified COD came off in the pH-3 fraction.

Through a technique of stripping dissolved ammonia, followed by preparation of o-phthalaldehyde derivatives, it was shown that amino acids are not present in detectable quantities. This result is significant because amino acids would fit several other characteristics of dissolved organic nitrogen that have been observed—low volatility, ionization at low pH, and difficult extractability.

The technique of evaporation to dryness yielded the degree of fractionation shown in Table 1. Nitrogen and sulfur compounds concentrate in the solids and redissolve in acetone to a large extent. The unidentified COD is largely present in the solid residue. Phenol and alkylated phenols enter the vapor and hence the condensate to a very large degree. This is therefore an effective method for removing the phenolics present in the highest concentrations, which would otherwise interfere with analyses for components present at lower concentrations.

Table 1. Fractionation between condensed vapor and solid residue (METC run 101 condensate water).

Compound	Concentration (mg/L)		
	Redissolved solids	Condensed product	METC run 101 condensate
Phenol	31	1260	1220
Cresols	17	1540	1510
Xylenols	56	1260	1260
Resorcinol	65	0	62
Pyrocatechol	51	0	41
Hydroquinone	4	0	6
4-Methyl catechol	39	0	36
5,5-Dimethyl hydantoin	112	0	108
COD	2110	10530	12250
Organic N	173	0	140
Organic S	404[b]	179[b]	404

[a]All concentrations corrected to the initial volume of the water sample.
[b]Samples were not stripped at low pH to remove hydrogen sulfide.

Liquid chromatographic (HPLC) analysis of the redissolved solids using a μ-Bondapak column and an aqueous mobile phase has shown that the unidentified COD concentrates in the earliest and latest portions of the chromatogram. Initial attempts to carry out analyses of HPLC fractions by gas chromatography/mass spectrometry (GS/MS) were complicated by bleeding of alkyl silanes from the stationary phase. This has since been cured by buffering at low pH.

Compounds identified for the first time in METC run 101 condensate water during FY 1984 include alpha- and beta-naphthalenol, aniline, and N-methyl formamide. Analytical accomplishments of previous years have been summarized in a manuscript.[1]

Extraction of Phenols with Trioctyl Phosphine Oxide (TOPO)

The results from previous years have been assessed to determine the conditions under which extraction with TOPO is most likely to be attractive in comparison with diisopropyl ether (DIPE) or methyl isobutyl ketone (MIBK). Extraction with TOPO-containing solvents can be carried out with substantially lower solvent-to-water flow ratios than is possible with MIBK or DIPE if the concentration of phenol in the feed water is 3000 ppm or less. Extraction with TOPO-containing solvents should also be considered for removal of di- and trihydroxybenzenes, in which case regeneration will probably have to be by a back-extraction method.

A manuscript[2] has been prepared on this portion of the work.

Recovery and Isolation of Ammonia through Simultaneous Extraction and Stripping

The experimental results obtained with di-2-ethylhexyl phosphoric acid (D2EHPA) in diluents composed of alkanes, aromatics, amines, and/or alcohols have been subjected to conceptual design analyses, which show that the use of amine diluents is preferred. There is a strong economic incentive for identification of acid extractants that have greater thermal stability than D2EHPA, since such extractants would allow regeneration with less steam consumption. A somewhat weaker organic acid would also be useful.

A full report[3] has been prepared on this phase of the work, along with a summary manuscript.[4]

Formation of Hydantoin Compounds

A literature search was conducted, using computer data bases covering the years 1967–1983. Very little information on the kinetics of hydantoin formation was uncovered.

Analytical methods were developed for following the disappearance of reactants and the formation of 5,5-dimethyl hydantoin (DMH). These include the use of specific-gas electrodes for carbon dioxide and ammonia, a specific-ion electrode for cyanide, gas chromatography for acetone, and HPLC for DMH.

Preliminary data for synthetic solutions for the most part sustain the Bucherer-Bergs reaction (acetone + carbon dioxide + ammonia + cyanide) as the principal formation mechanism for 5,5-dimethyl hydantoin. Relatively smooth kinetic data have been obtained, so far supporting second-order kinetics when ammonia and carbon dioxide are present in large excess. However, in early results the reactants do not disappear in stoichiometric proportion, nor does DMH appear stoichiometrically. Possible reasons for this are being investigated.

Synfuels Wastewater Workshop

The proceedings of the 1983 Morgantown Synfuels Wastewater Workshop have been published.[5]

PLANNED ACTIVITIES FOR FY 1985

Analyses will be continued for the HPLC fractions obtained from redissolved residual solids from evaporation of condensate water. The anhydrous and concentrated nature of these samples makes them well suited for GC/MS analysis. These investi-

gations will be supplemented by pH-gradient fractionation, analyses of organic nitrogen and organic sulfur, and other techniques. Adsorption with functionalized resins or carbons will also be explored, both as a complementary method of fractionation among solutes and as a potentially useful processing method. Total organic carbon (TOC) measurements, when available, will be used to supplement COD measurements and to determine the degree of oxidation of various fractions.

Measurements will be made of *in situ* equilibrium distribution coefficients of the compounds present in condensate water. These will reveal complexation, micellization, adsorption onto suspended solids, or other complicating factors within the waters.

Measurements of the mechanism, kinetics, and formation of 5,5-dimethyl hydantoin in synthetic solution and in condensate waters will be continued in an effort to ascertain the reaction mechanism, possible side reactions and complications, and important parameters in quench-circuit design relating to hydantoin formation. It is anticipated that this phase of the work will be concluded during FY 1985.

An attractive possibility is to combine the extraction-based method for recovery and isolation of ammonia with the removal of organics by the same extraction system. This potentially important synergism will be examined through experiments and process calculations. Extraction of heavy phenolics or other substances might contaminate a cation-exchanging extractant such as D2EHPA. The use of a cation-exchange polymeric resin will be explored as a method for keeping the ammonia-removal extractant separate from the organics-extraction system. In the latter case, the potential synergism would lie in the ability to use one and the same steam-heated column to regenerate the solvent and to remove the ammonia thermally from the resin.

Cation-exchanging extractants more stable thermally than D2EHPA and/or somewhat weaker in acidity will be sought in an effort to reduce the steam consumption needed to regenerate ammonia thermally from such an extractant.

Computer simulations of ammonia and acid-gas stripping will also be initiated so as to give insight into other avenues that may be effective in reducing the energy requirement for removal and isolation of ammonia.

REFERENCES

1. Mohr, D.H. and King, C.J. (1984), *Identification and Separation of the Organic Compounds in Condensate Waters from a Coal-Gasification Process,* LBL-17319.
2. MacGlashan, J.D., Bixby, J.L., and King, C.J. (1984), "Separation of Phenols from Dilute Aqueous Solutions by Use of Tri-n-Octyl Phosphine Oxide as Extractant," *Solvent Extr. and Ion Exch.* (in press); LBL-18378.
3. Mackenzie, P.D. and King, C.J. (1984), *Simultaneous Stripping and Solvent Extraction for the Recovery of Ammonia and Acid Gases from Wastewaters*, LBL-17740.
4. Mackenzie, P.D. and King, C.J., (1984), "Combined Solvent Extraction and Stripping for Removal and Isolation of Ammonia from Sour Waters," *Ind. Eng. Chem. Process Des. & Devel.* (in press); LBL-18099.
5. King, C.J., Ed. (1984), *Proceedings of the Third Biennial Synfuels Wastewater Workshop,* DOE/METC/85-5 (DE84009294), Morgantown Energy Technology Center, Morgantown, WV.

Separations of Polar Organics from Aqueous Solutions by Processes Based upon Reversible Chemical Complexation*

C.J. King, A.S. Kertes, D. Arenson, and J. Tamada

Industrial separations of polar organic substances from water are carried out for the most part by distillation or evaporation. They thereby consume a large amount of energy.[1] This is especially true for substances such as acetic acid, glycols, sugars, cornstarch products, and other hydrophilic substances that are less volatile than water. Separations of this type are becoming more and more important with the advent of biological production of chemicals and the need for improved cleanup of effluent streams.

Solvent extraction with reversible complexing agents ("extractants") is a promising alternative separation method. If a high degree of concentration of the solute can be obtained in the extract through a large equilibrium distribution coefficient, the energy requirement for regeneration of the extractant will be substantially less than that for distillation or evaporation. In addition to giving high distribution coefficients for dilute solutes, chemically complexing extractants can provide high selectivity for the solute(s) of interest, by virtue of their chemical specificity.[2]

The purpose of this project is to examine and evaluate the use of reversible chemical complexation as a method for large-scale separation of polar organic substances from aqueous solution. Solutes of particular interest in the initial portion of the project are carboxylic acids, alcohols, and difunctional compounds containing these groups. Emphasis is on the use of purely organic extractants, rather than those containing metals.

ACCOMPLISHMENTS DURING FY 1984

This project was started in July 1984. A principal activity in the initial phase has been a literature survey on solvent-extraction chemistry for carboxylic acids involved in the pyruvic/tricarboxylic cycle of glucose fermentation. These include lactic, succinic, tartaric, propionic and citric acids—all major chemical products—as well as pyruvic, furmaric, maleic, malic, and itaconic acids.

A survey of the literature on hydrogen bonding with alcohols indicates that phosphoryl substances, notably phosphine oxides, may be attractive as extractants. From past studies, we know that tertiary amines, and also phosphoryl compounds, are effective for extraction of carboxylic acids. These solute/extractant systems were selected for initial study.

Analytical methods for different carboxylic acid solutes have been evaluated, in particular those based upon differential interferometry and gas chromatography.

PLANNED ACTIVITIES FOR FY 1985

The literature survey on extraction of fermentation acids will be completed, presented at the annual American Chemical Society meeting, and submitted for publication.

On the bases of commercial importance, ease of chemical analysis, and solute stability, a dicarboxylic acid and a hydroxycarboxylic acid will be selected for initial extraction studies, to be made with tertiary amines and phosphine oxides in candidate diluents.

Phase equilibrium characteristics will be measured for extraction of alcohols (e.g., butanol, ethanol) with phosphoryl extractants. Initially, trioctyl phosphine oxide, an important extractant from the metals industry, will be used. It is anticipated that the choice of diluent will be very important and may exert a controlling influence on solute extractability.

Regeneration studies will be carried out along with the extraction studies. The principal methods of regeneration to be considered initially are distillation and back-extraction into an aqueous phase, following an appropriate change in conditions.

REFERENCES

1. Mix, T.W., Dweck, J.S., Weinberg, M., and Armstrong, R.C. (1974), "Energy Conservation in Distillation," *Chem. Eng. Progr. 74* (4), p. 49.
2. King, C.J. (1983), "Separation Processes Based upon Reversible Chemical Complexation," plenary lecture at the Tenth Interamerican Congress of Chemical Engineering, Santiago, Chile, November 1983.

*This work was supported by the Assistant Secretary for Conservation and Renewable Energy, Office of Energy Systems Research, Energy Conservation and Utilization Technologies Division of the U.S. Department of Energy under Contract No. DE-AC03-76SF00098.

Dynamics Of Liquid Filament Breakup*

D.W. Bousfield, G. Marrucci, and M.M. Denn

The breakup of a liquid filament into droplets is an important step in a variety of processes, including, for example, coal liquefaction; applications in a wide range of industries have recently been enumerated by Schümmer and Tebel.[1] The mechanisms governing the early stages of the breakup of Newtonian jets appear to be generally understood.[2,3] This is not the case for viscoelastic jets; it has been observed experimentally that jets of polymer solutions generally take longer to break up into droplets than do purely viscous jets of comparable viscosity, and sometimes do not break up at all, although existing theory for the stability of viscoelastic filaments predicts a more rapid growth of disturbances.[4-6]

We show here the results of a dynamical analysis of the growth of surface tension–driven disturbances on thin filaments of Newtonian and Maxwellian liquids, using a one-dimensional approximation analogous to that developed for the analysis of fiber spinning.[7] The results are consistent with linear stability analyses during the initial portion of the transient, but they also enable calculations at long times approaching breakup. Nonlinearities associated with inertial stresses cause the formation of satellite droplets in Newtonian jets that have been observed experimentally.[8] The retardation of disturbance growth and the stabilization of viscoelastic jets at long times are shown to be a consequence of nonlinearities associated with the buildup of large extensional stresses. An asymptotic analysis of long times points up the essential differences in nonlinear disturbance growth between purely viscous and viscoelastic filaments.

ACCOMPLISHMENTS DURING FY 1984

One-Dimensional Analysis

The basic assumption of this analysis is that the wavelength of a disturbance remains constant in time as a surface tension–driven disturbance grows and droplets form. This assumption is based on photographic evidence of the breakup of filaments forced with a constant frequency.[5,8] The momentum equation at each position in a thin Newtonian filament, averaged over the filament cross section and neglecting radial momentum, is then:

$$\dot{r} = \left(\frac{1}{r} + \frac{\alpha^2 r_{\zeta\zeta}}{(1+\alpha^2 r_\zeta^2)}\right)\frac{r}{6(1+\alpha^2 r_\zeta^2)^{1/2}} - \frac{1}{6r}\int_0^\zeta \beta \dot{u} r^2 d\zeta - \frac{F}{r} \quad , \tag{1}$$

$$F = \frac{\int_0^1 \left(\frac{1}{r} + \frac{\alpha^2 r_{\zeta\zeta}}{(1+\alpha^2 r_\zeta^2)}\right)(1+\alpha^2 r_\zeta^2)^{-1/2} d\zeta - \int_0^1 \frac{1}{r^2}\left(\int_0^\zeta \beta \dot{u} r^2 d\zeta\right) d\zeta}{6\int_0^1 r^{-2} d\zeta} \quad , \tag{2}$$

$$\dot{r} = r_\theta + u r_\zeta \quad , \tag{3}$$

$$\dot{u} = u_\theta + u u_\zeta \quad , \tag{4}$$

$$u = -2\int_0^\zeta r^{-1}\dot{r} d\zeta \quad . \tag{5}$$

*This work was supported by the Director, Office of Energy Research, Office of Basic Energy Sciences, Materials Sciences Division of the U.S. Department of Energy under Contract No. DE-AC03-76SF00098, and by the U.S. Army, ARRADCOM, under Agreement No. 3311-1412.

Here the dimensionless variables are $r = R/R_o$, $\zeta = z/L$, and $\theta = \sigma t/\eta R_o$, where R and R_o are the radius and initial radius of the filament, respectively; z is position; L is half the disturbance wavelength; t is time; and σ and η are the liquid surface tension and viscosity, respectively. Subscripts denote partial differentiation. The parameters α and β are defined as

$$\alpha = R_o/L \quad ,$$

$$\beta = \left(\frac{\rho\sigma R_o}{\eta^2}\right)\left(\frac{L}{R_o}\right)^2 ,$$

where ρ is the density, and the dimensionless group $\eta^2/\rho\sigma R_o$ is the square of the Ohnesorge number. The limit of negligible inertia is obtained for $\beta = 0$, while the equations appropriate for small curvature follow by taking $\alpha = 0$. Small curvature with negligible inertia requires that $\rho\sigma R_o/\eta^2$ go to zero more rapidly than α^2.

For a Maxwell fluid, we record the thin-filament equations analogous to Eqs. (1) and (2) only in the limit $\alpha = 0$, $\beta = 0$, since this is the only form for which computational results have been obtained:

$$\dot{r} = \frac{\psi - r^2(\tau_{11}-\tau_{22})}{2r\phi(\tau_{11}+2\tau_{22}) + 6r - \phi} \quad , \tag{6}$$

$$\psi = \frac{\int_0^1 \frac{r^2(\tau_{11}-\tau_{22})d\zeta}{2r^2\phi(\tau_{11}+2\tau_{22}) + 6r^2 - r\phi}}{\int_0^1 \frac{d\zeta}{2r^2\phi(\tau_{11}+2\tau_{22}) + 6r^2 - r\phi}} \quad , \tag{7}$$

where τ_{11} and τ_{22} are the axial and radial components of the extra stress, normalized with respect to $\sigma/\eta R_o$. The viscoelastic parameter ϕ is defined as

$$\phi = \lambda\sigma/\eta R_o \quad ,$$

where λ is the Maxwellian relaxation time.

It has been observed experimentally that at long times the viscoelastic filament approaches a configuration approximated by a long cylinder of uniform radius connecting two large droplets. The pressure in the droplets can be taken to be close to atmospheric, in which case the radius of the cylinder decreases uniformly according to the equation:

$$\phi\frac{\ddot{r}}{\dot{r}} + 9\phi^2\left(\frac{\dot{r}}{r}\right)^2 - \phi\frac{\dot{r}}{r} - 6\dot{r} - 1 = 0 \quad . \tag{8}$$

Equation (8) is equivalent to a special case of Eq. (66) of Schümmer and Tebel.[1] The Newtonian fluid is recovered in the limit of no elasticity:

$$\phi \to 0 : r = constant - \theta/6 \quad . \tag{9}$$

For $\theta >> \phi$, the asymptotic behavior for a Maxwell fluid follows as

$$\theta >> \phi : \ln r = constant - \theta/3\phi \quad . \tag{10}$$

It is clear from this asymptotic behavior that a Newtonian filament in this configuration would rupture in a finite time of order $\theta = 6$ ($t = 6\eta R_o/\sigma$), while a viscoelastic filament would thin much more slowly; the exponential approaches zero for $\theta \approx 9\phi$, corresponding to $t \approx 9\lambda$. Viscoelastic effects will therefore dominate if $\phi >> 1$.

The initial growth rate in the absence of inertia is available analytically from the linear stability theory of Middleman.[6] This can be expressed as

$$\ln(r-1) = \ln[r(o)-1] + \frac{\theta}{6-\phi} \quad . \tag{11}$$

Numerical Results

Equations (1) and (2) or (6) and (7) are readily solved by a straightfoward procedure of marching in time at each spatial position, with all spatial derivatives and integrals evaluated at the start of the time step. Initial conditions were taken to correspond to a small sinusoidal perturbation about a uniform cylinder to facilitate comparison with results from linear stability theory. In accordance with the stability theory, a disturbance will grow on a Newtonian filament only for $\alpha < 1/\pi$ and on a Maxwellian filament in the absence of inertia only for $\phi < 6$.

Profile development with time is shown in Figs. 1 and 2 for a Newtonian filament with $\alpha = 0.1$; $\beta = 0$ in Fig. 1 corresponds to a very viscous liquid, and $\beta = 1080$ in Fig. 2 is typical of a glycerine-water solution. The disturbance grows most rapidly for the viscous liquid at the midpoint between the developing droplets. The effect of inertia is to cause the most rapid growth to occur close to the droplet during the latter stages of breakup, leading to the breaking off of a large droplet from a thin ligament; this nonlinearity is the source of the satellite droplets observed in experiments with glycerine-water solutions by Goedde and Yuen.[8]

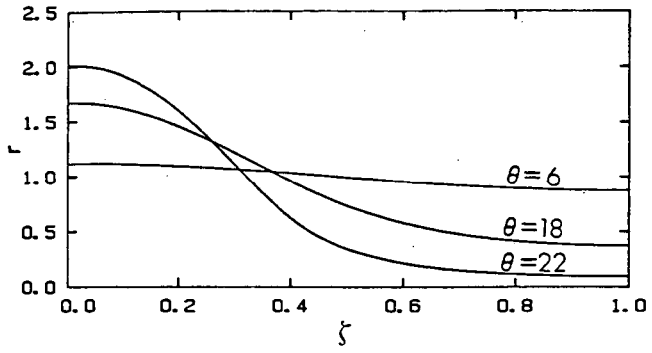

Figure 1. Profile progression for a Newtonian filament; $\alpha = 0.1$, $\beta = 0$. (XBL 853-1844)

Profile development with time is shown in Fig. 3 for a Maxwell fluid with $\phi = 2$. The growth rate of the disturbance is initially more rapid than for a viscous Newtonian fluid, in accordance with linear stability theory; at longer times, the growth is retarded, and the filament approaches a configuration corresponding to a long cylinder connecting two large droplets, the configuration described by Eq. (8). The calculations were stopped when a theory of small curvature ($\alpha = 0$) became clearly inadequate.

Comparison between the growth of a disturbance on viscous Newtonian and Maxwellian filaments is facilitated in Fig. 4, where the diameter of the filament midpoint (the thinnest point) is plotted versus time. The broken lines shown in the figure represent Middleman's linear stability theory, Eq. (11). There is a qualitative change in the thinning of the viscoelastic filament at long times, with an asymptotic approach to breakup described by Eq. (10); in contrast, the Newtonian filament breaks up in a finite time.

The stabilization of jets of polymer solutions is usually attributed to resistance to extensional deformations.[5] The computed stretch rate Γ_e at $\zeta = 0.4$ for the viscoelastic filaments is shown in Fig. 5. Clearly the stabilization at long times corresponds to the rapid growth of $\lambda\Gamma_e$, which is consistent with the known extensional behavior of Maxwellian liquids.[9] It is this nonlinear behavior resulting from the buildup of extensional stresses that inhibits the breakup of the viscoelastic jets. Inclusion of a finite tensile stress at $t = 0$ to account for the residual stress of exiting the nozzle, as in the linear stability analysis of Goren and Gottlieb,[10] retards the initial disturbance growth but has little qualitative effect on the ultimate nonlinear behavior.

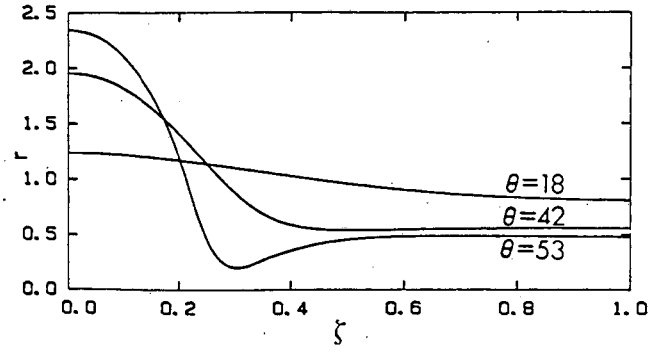

Figure 2. Profile progression for a Newtonian filament; $\alpha = 0.1$, $\beta = 1080$. (XBL 853-1845)

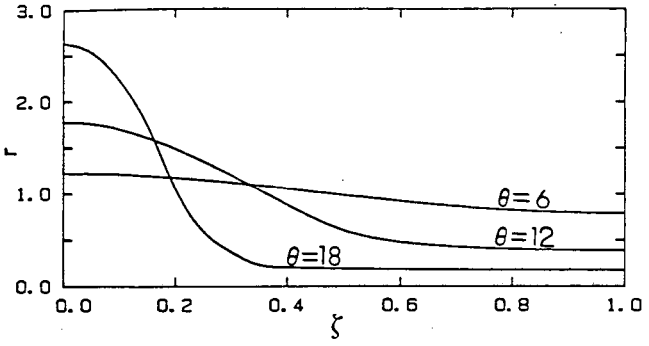

Figure 3. Profile progression for a Maxwell fluid filament; $\alpha = 0.1$, $\beta = 0$, $\phi = 2$. (XBL 853-1846)

Conclusion

This one-dimensional analysis explains the important experimentally observed features of filament breakup, including the initial linear growth, the formation of satellite droplets, and the retarded breakup of viscoelastic jets. The calculations are in good quantitative agreement with the detailed tran-

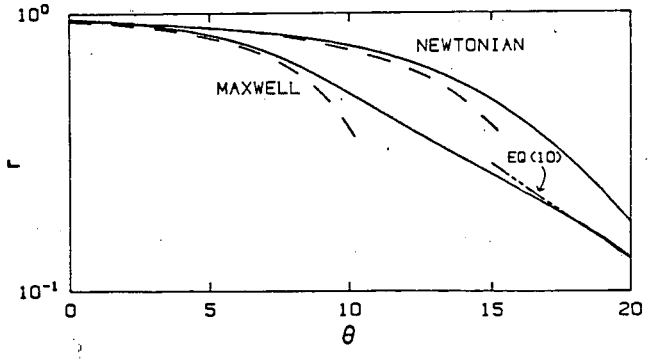

Figure 4. Filament midpoint radius as a function of time, $\alpha = 0.1$, $\beta = 0$, for a Newtonian fluid and a Maxwell fluid with $\phi = 2$. Broken lines are from the linear stability analysis, Eq. (11). (XBL 853-1847)

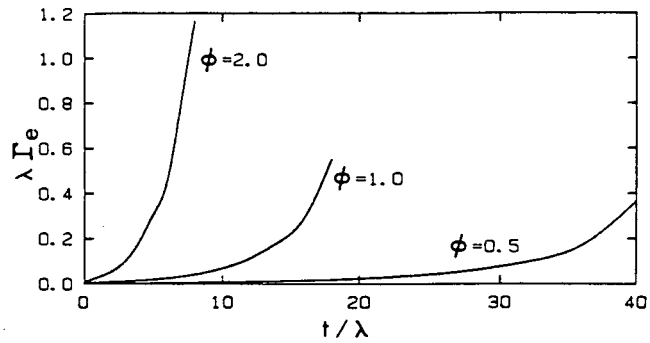

Figure 5. Dimensionless stretch rate ($\lambda\Gamma_e$) vs. dimensionless time (t/λ) at $\zeta = 0.4$ for a Maxwell fluid, $\alpha = 0$, $\beta = 0$. (XBL 853-1843)

sient finite-element calculations carried out by Keunings,[11] and the method therefore provides an effective, low-cost means of studying the effect of rheological properties and disturbance initiation on filament stability and breakup.

PLANNED ACTIVITIES FOR FY 1985

The one-dimensional analysis will be extended to represent an Oldroyd-B fluid, including inertial effects, in order to compare theory with experimental results. The behavior of a void in extensional flow will also be studied.

REFERENCES

1. Schümmer, P. and Tebel, K.H. (1982), "Production of Monodispersed Drops by Forced Disturbance of a Free Jet," *German Chem. Eng. 5,* p. 209.
2. Bogy, D.B. (1979), "Drop Formation in a Circular Liquid Set," *Ann. Rev. Fluid Mech. 11,* p. 207.
3. McCarthy, M.J. and Molloy, N.A. (1974), "Review of Stability of Liquid Jets and the Influence of Nozzle Design," *Chem. Eng. J. 7,* p. 1.
4. Goldin, M., Yerushalmi, J., Pfeffer, R., and Shinnar, R. (1969), "Stability of Viscoelastic Capillary Jets," *J. Fluid Mech. 38,* p. 689.
5. Gordon, M., Yerushalmi, J., and Shinnar, R. (1973), "Instability of Jets of Non-Newtonian Fluids," *Trans. Soc. Rheol. 17,* p. 303.
6. Middleman, S. (1965), "Stability of a Viscoelastic Jet," *Chem. Eng. Sci. 20,* p. 1037.
7. Denn, M.M. (1980), "Continuous Drawing of Liquid to Form Fibers," *Ann. Rev. Fluid Mech. 12,* p. 365.
8. Goedde, E.F., and Yuen, M.C. (1970), "Experiments on Liquid Jet Instability," *J. Fluid Mech. 40,* p. 495.
9. Denn, M.M. and Marrucci, G. (1971), "Stretching of Viscoelastic Liquids," *AIChE J. 17,* p.101.
10. Goren, S.L. and Gottlieb, M. (1982), "Surface-Tension-Driven Breakup of Viscoelastic Liquid Threads," *J. Fluid Mech. 120,* p. 245.
11. Keunings, R. (1984), "A Finite Element Method for a Class of Viscoelastic Flows in Deforming Domains Applied to Jet Breakup," *Proc. IX Intl. Congress on Rheology 1,* p. 699.

Removal of H_2S from Coal-Derived Synthesis Gas*

S. Lynn, R. Demyanovich, D. Neumann, and S. Sciamanna

When coal is gasified, most of the organic sulfur is converted to hydrogen sulfide. The problem of removing hydrogen sulfide varies with the nature and proposed use of the gas produced. In some cases, one wishes to remove only hydrogen sulfide; in others, carbon dioxide must be removed as well; and in still other cases, there are hydrocarbons that can profitably be recovered as separate products. Conventional technology for removing H_2S from a gas stream consists of

- passing the gas through an absorber where H_2S (and, to a large extent, CO_2) is absorbed in an aqueous solution of an ethanol amine or potassium carbonate;
- stripping the dissolved gas from solution with steam;
- burning a third of the H_2S with air to form SO_2 and generating steam with the released energy in a waste-heat boiler;
- passing the mixture of SO_2 and H_2S through a succession of fixed-bed reactors,

*This work was supported by the Assistant Secretary for Fossil Energy, Office of Coal Utilization Systems, Division of Surface Coal Gasification, of the U.S. Department of Energy under Contract No. DE-AC03-76SF00098.

- cooling the gas stream between reactors to condense sulfur; and
- sending the tail gas from the process above (a Claus sulfur plant) to one of a variety of processes to deal with the unreacted 5% of sulfur compounds.

A new process, which has been under development at the Lawrence Berkeley Laboratory since January 1, 1984, substitutes these features:

- absorbing the H_2S and, optionally, other gases in a polar organic solvent;
- converting the dissolved H_2S to sulfur by reacting it with an equivalent amount of SO_2 dissolved in the same solvent;
- recovering co-absorbed gases from the solvent by stripping;
- recovering elemental sulfur from the solvent by crystallization; and
- generating the SO_2 for the process by burning H_2S or sulfur, recovering heat from the combustion gas in a waste-heat boiler, and recovering SO_2 by scrubbing the gas with cooled solvent from the crystallization step.

A flowsheet for one embodiment of this process is shown in Fig. 1. This application is designed for desulfurizing synthesis gas (a mixture of hydrogen and carbon monoxide, with carbon dioxide, water vapor and hydrogen sulfide as undesirable impurities), one of the most likely products of coal gasification. The process removes the three impurities from the synthesis gas simultaneously in a single absorption step (reducing H_2S to the parts-per-million level), converts the hydrogen sulfide to sulfur, and produces a sulfur-free stream of carbon dioxide as a byproduct.

This process promises to lower capital and operating costs, to reduce both energy consumption and emissions of atmospheric pollutants, and to have greater flexibility and selectivity than the conventional technology for acid gas removal.

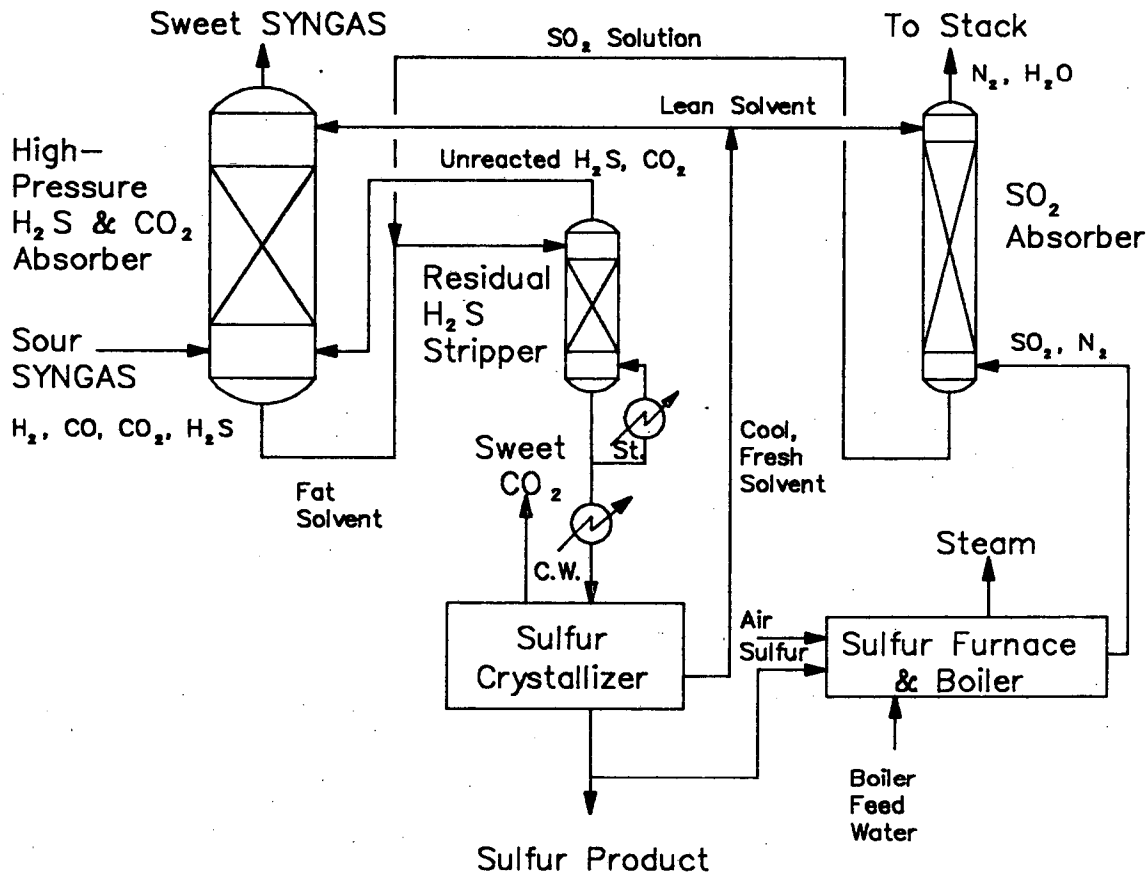

Figure 1. Removal of H_2S from coal-derived synthesis gas. (XBL 851-944)

ACCOMPLISHMENTS DURING FY 1984

The work of this project has been divided into the following tasks:

(1) Determine the solubilities of H_2S, SO_2, CO_2, CH_4 and other hydrocarbon gases, water, and sulfur in the organic solvent as functions of pressure, temperature, and solvent composition.
(2) Determine the effects of temperature and solvent composition on reaction kinetics.
(3) Investigate the suitability of steel and other materials of construction for this system.
(4) Set up a computer model of this process to aid in its evaluation and evolution.
(5) Compare the anticipated costs of this process with those of conventional technology.

The first gas-solubility measurements have been made for sulfur dioxide in a variety of solvents. Figure 2 shows some of the data for 75°C. These data have been correlated with various theories taken from the literature to facilitate subsequent calculation of process behavior. The solid curves show the correlation of the data with UNIQUAC* for SO_2 in pure N,N-dimethyl aniline (DMA) and pure diethylene glycol–methyl ether (DGM or carbitol), and the dashed curves show the UNIFAC* predictions of the solubility of SO_2 in mixtures of DMA and DGM. Figure 3 shows solubility data for SO_2 in a wide variety of solvents at 50°C. The work on SO_2 solubility was completed during the summer of 1984. New equipment has been constructed to measure the solubilities of the other gases of interest, which are lower by factors of 10 to 100 than the solubility of SO_2.

Sulfur solubility in mixtures of DMA and DGM is shown in Fig. 4 as functions of temperature and composition. These solubility determinations are made as follows: weighed samples of sulfur and solvent are first heated until the sulfur dissolves, then the solution is then cooled to precipitate fresh sulfur crystals, and finally the mixture is reheated until the crystals just redissolve. The heating during the third step must be done relatively slowly to ensure that the temperature obtained is that for true equilibrium. The effect of water as well as various organic compounds on sulfur solubility is being determined. These solutions are highly nonideal, and the best method of correlating the data is still to be determined.

*UNIQUAC and UNIFAC are well-known methods of correlating vapor-liquid equilibrium data and of predicting ternary behavior from binary data. These methods were developed by J.M. Prausnitz and his co-workers.

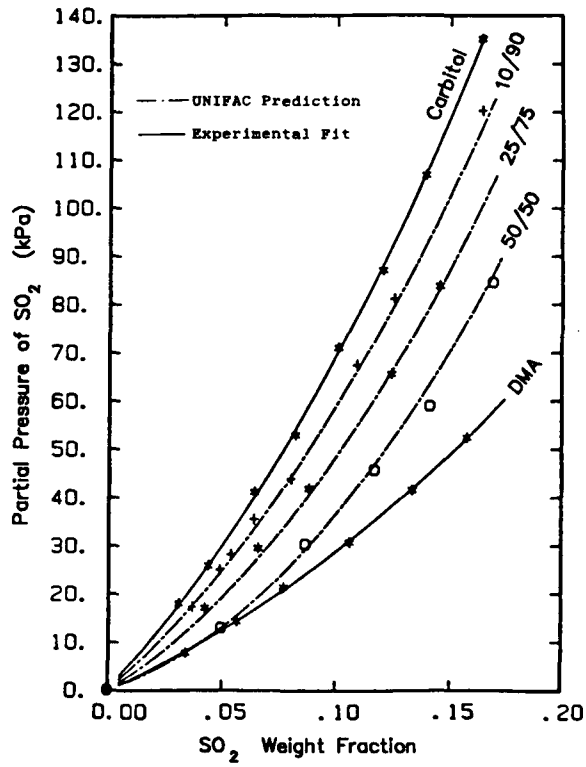

Figure 2. Comparison of UNIFAC predictions with experimental data for the partial pressure of SO_2 in mixtures of DMA and carbitol (DMG) at 75°C. (XBL 851-945)

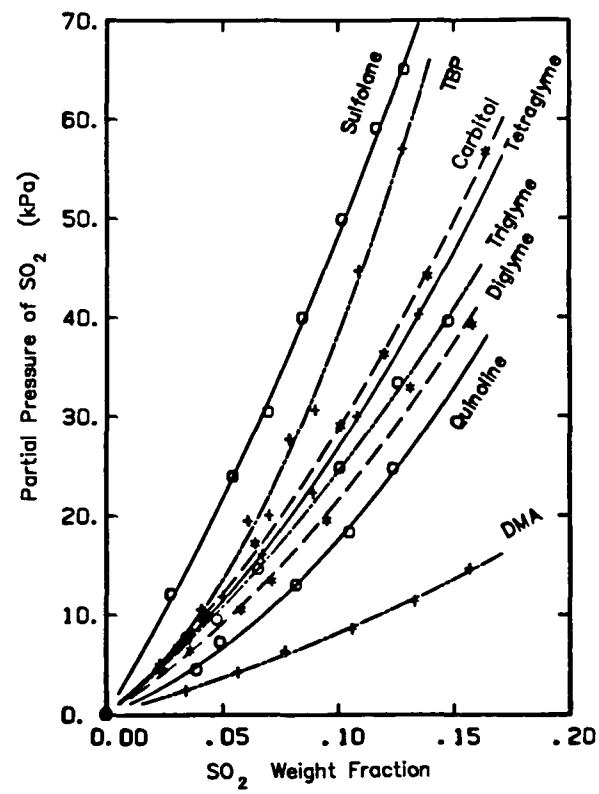

Figure 3. Vapor-liquid equilibria of SO_2 in organic solvents at 50°C. (XBL 851-946)

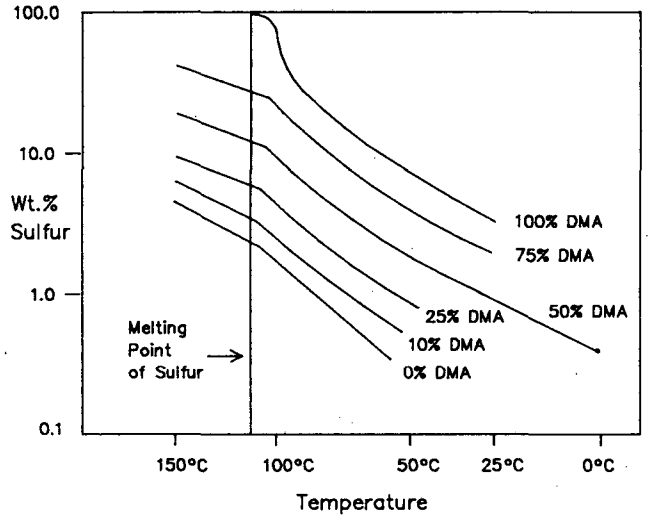

Figure 4. Sulfur solubility in mixtures of DMA and DGM. (XBL 851-947)

Kinetic studies in this system are performed with the simple calorimeter shown in Fig. 5. A weighed sample of solvent containing H_2O is placed in the calorimeter together with a magnetic stirring bar and a bare thermocouple. A weighed sample of solvent containing SO_2 is added rapidly while stirring vigorously, and the potential of the thermocouple is recorded as a function of time. These potential readings are converted to temperatures, which in turn are related to changes in concentration of the H_2S and SO_2. From these data, the order of the reaction and its rate can be determined. The reaction has been found to be first order with respect to both H_2S and SO_2. Values of the reaction rate constant, k_2, of less than 1 L/mole-s have been found in both mono- and dialkyl ethers, of ethylene glycols. The addition of DMA to either type of solvent catalyzes the reaction. In the dialkyl ethers the addition of water or an alcohol enhances the catalytic effect of the DMA. These results, from reactions carried out at ambient temperature, are shown in Fig. 6 and 7. This enhancement appears to be produced by the hydroxyl group in water and alcohols, which is of course also present in monoalkyl ethers of the ethylene glycols. From experiments performed at about 10°C, the activation energy for the reaction is estimated to be about 7.4 kcal/mole, which corresponds to a doubling of the rate every 20°C. For values of k_2 greater than 15, the reaction reaches more than 90% completion in less than 5 seconds, and the precision of estimating k_2 becomes increasingly poor. A different measurement technique will therefore be needed to make accurate estimates of k_2 at temperatures much above ambient.

Preliminary estimates of the capital and operating costs of this process indicated that both would be significantly lower than those for conventional technology if no technical complications were encountered. The results to date have been reassuring. The proposed solvent consists primarily of polyglycol ethers and is similar in properties to solvents in current commercial use. The solubilities of the various gases and of sulfur in this solvent could be approximated for the preliminary estimates and are now being measured. The experimental values do not vary greatly from the estimates. The kinetics of the reaction between H_2S and SO_2 in the solvent is so fast that no reaction volume need be allowed to ensure its completion—the process piping itself provides the needed residence time. In the experiments done to

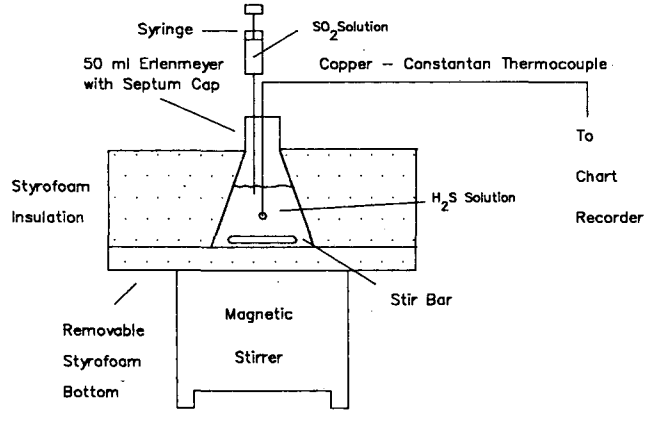

Figure 5. Experimental apparatus for kinetic studies of SO_2 and H_2S in solution. (XBL 851-948)

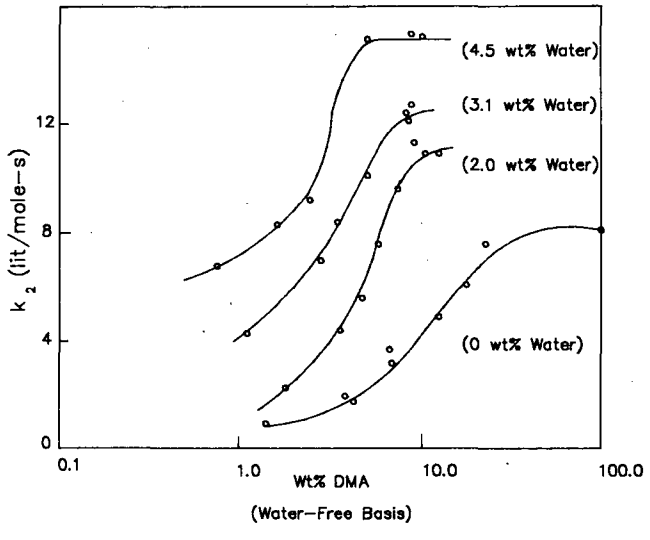

Figure 6. Variation of second-order rate constant with DMA and water content in triglyme. (XBL 851-949)

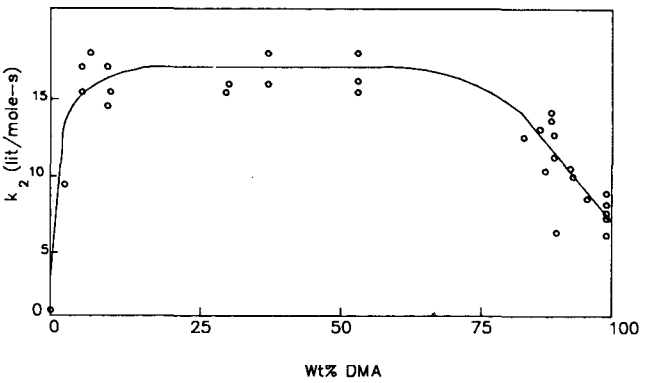

Figure 7. Variation of second-order rate constant with wt% DMA for DMA in DGM at 17°–23°C (no water).
(XBL 851-950)

date, there have been no indications of the presence of any sulfoxy compounds (thiosulfate, dithionite, polythionates, etc.) of the sort that form when H_2S and SO_2 react in aqueous solution. Such compounds are highly acidic and require neutralization with sodium carbonate or some other base. Their absence relieves this process of a serious complication. The experimental program is intended to investigate and resolve all questions of technical feasibility as they arise as well as to obtain the physical and chemical data needed for design.

PLANNED ACTIVITIES FOR FY 1985

Three of the tasks described above are scheduled to be started in FY 1985. These are the determination of materials compatibility, the development of a computer program to simulate the steady-state operation of the process, and the estimation of capital and operating costs for the process in comparison with those for conventional technology. In performing the latter two tasks, it is planned to evaluate the performance of the process in treating several different hydrogen sulfide–containing gas streams of industrial importance, since the presence of H_2S is a problem that arises in the processing of many fuels.

A waste-gas stream of significant industrial interest is the tail gas from a Claus process sulfur plant. This gas contains both hydrogen sulfide and sulfur dioxide in a molar ratio of about two to one and at concentrations of several thousand parts per million. To use the present process to desulfurize Claus tail gas would require absorbing both H_2S and SO_2 simultaneously, even as the reaction between the two is occurring. The theory for this type of absorption-with-chemical reaction is not well developed. The study of this problem will involve both the experimental determination of absorption behavior and the mathematical modeling of the system. The results should also be of interest for estimating the effect of adding SO_2 to the solvent in a high-pressure absorption step in order to reduce the H_2S concentration in the gas being treated to an exceptionally low level.

The ultimate objective of this work is the development of an improved, flexible process for desulfurizing gasified coal and other sour gas streams. At this point in the project, this objective appears to be feasible.

ELECTROCHEMICAL ENERGY STORAGE RESEARCH

Technology Base Research Project for Electrochemical Energy Storage*

E.J. Cairns, K. Kinoshita, and F.R. McLarnon

The Lawrence Berkeley Laboratory (LBL) is lead center for management of the Technology Base Research (TBR) Project, which is supported by the Electrochemical Branch of DOE's Energy Storage Division. The purpose of this project is to provide the research base to support DOE efforts to develop electrochemical energy conversion systems for electric vehicle and stationary energy storage applications. The specific goal is to identify the most promising electrochemical technologies and transfer them to industry and/or another DOE program for further development and scale-up.

The TBR project is divided into four major project elements: electrochemical systems, supporting research, electrochemical processes, and fuel cell research. The generic research topics included in each of these elements are listed in Table 1.

General research areas addressed by the TBR Project include identification of new electrochemical couples for advanced batteries, determination of technical feasibility of the new couples, improvements in battery components and materials, establishment of engineering principles applicable to electrochemical energy storage and conversion, and the investigation of fuel cell and metal/air systems for transportation applications. Major emphasis of the project is given to applied research that will lead to superior performance and lower life-cycle costs.

The LBL scientists participating in the program are E.J. Cairns, K. Kinoshita, and F.R. McLarnon of the Applied Science Division, and L.C. DeJonghe, J.W. Evans, R.H. Muller, J.S. Newman, P.N. Ross, and C.W. Tobias of the Materials and Molecular Research Division.

Table 1. Topics covered by the technology base research project for electrochemical energy storage.

I. ELECTROCHEMICAL SYSTEMS
- New Rechargeable Electrochemical Cells
- Metal/Air Cells

II. SUPPORTING RESEARCH

A. *Engineering-Science Research*
- Electrode Morphological Studies, Chemical/Structural Analysis
- Transport Phenomena, Electrocatalysis, Electrode Kinetics, and Cell Thermodynamics
- Modeling of Electrochemical Cells and Battery Systems
- Advanced Physicochemical Methods for Electrochemical Research

B. *Materials Research*
- Ceramic, Molten-Salt, Glass, and Polymeric Electrolytes
- Novel Electrode Structures
- New Component Fabrication Techniques
- Battery Separators

III. ELECTROCHEMICAL PROCESSES
- Corrosion Problems in Electrochemical Storage Devices
- Air Electrodes
- Thermally Regenerative Cells

IV. FUEL CELL RESEARCH
- New Components for Fuel Cells
- New Electrolytes
- Electrocatalysis

ACCOMPLISHMENTS DURING FY 1984

LBL conducted a vigorous in-house research program and monitored 36 subcontracts. A description of the research projects conducted by the subcontractors can be found in the recent annual report, *Technology Base Research Project for Electrochemical Energy Storage* (LBL-17742). The in-house work, "Electrochemical Energy Storage," is summarized in the next article and in the *Materials and Molecular Research Division FY 1984 Annual Report* (LBL-18570). Highlights of the subcontracted work follow.

*This work was supported by the Assistant Secretary for Conservation and Renewable Energy, Office of Energy Systems Research, Energy Storage Division of the U.S. Department of Energy under Contract No. DE-AC03-76SF00098.

Electrochemical Systems

- Duracell Inc. achieved 200–300 cycles (50% depth-of-discharge) to 2.6 V cutoff in their 2/3A-size Li/SO_2 cells (0.4–0.5 Ah) with theoretical specific energy of about 1100 Wh/kg.
- Case Western Reserve University has found that several combinations of tetramethoxyphenyl porphyrins (TMPP) containing various transition metals are even more active as O_2 reduction catalysts than H_2TMPP after pyrolysis at 450°C.
- An Al/air cell was operated by LLNL for 4.12 hours at 140 A (230 mA/cm_2). The supersaturated electrolyte and seed were transferred to a separate container for a batch crystallization experiment. The plastic hydrocyclone fabricated by LLNL gave good separation, with a d_{50} (separation factor indicating diameter at which 50% of particles are removed) of about 3.5 μm.

Supporting Research

- Pinnacle Research Institute has completed measurement of the hydraulic permeability of electrolyte and zincate-ion permeability through their hybrid separators. The hydraulic permeability varied from 1.74×10^{-7} to 6.66×10^{-7} mL-cm/s-cm^2-atm, and the zincate-ion permeability was 9.6×10^{-11} mole/cm^2-s. These results indicate that the hybrid separators have better selectivity and electrolyte transport properties than those of microporous separators.
- The application of supported-liquid membrane separators in alkaline Zn/NiOOH cells was successfully demonstrated by Castle Technology Corporation. This technology was transferred to the Exploratory Development and Testing Program at Sandia National Laboratories and is being tested in Zn/ferricyanide cells.
- LLNL has completed measurement of mutual diffusion coefficients for aqueous, high-purity $ZnCl_2$at 25.00° ± 0.005°C. These measurements are precise to 0.1–0.2% and cover the concentration range from 0.004996 to 7.2489 mol/(kg H_2O).
- Various Li-Al-Si alloy negative electrodes were studied by Argonne National Laboratory (ANL). Test results indicate that these electrodes have excellent capacity retention when cycled in the potential range −0.2 to 0.15 V versus Li-Al. The specific capacity (Ah/g) of an alloy with an Al to Si ratio of one was a factor of 1.4 to 1.5 greater than that for the Li-Al alloy.
- ANL has completed characterization of the nickel sulfide electrode. Two distinct reaction mechanisms appeared: (1) at 1.0–1.6 V versus Li-Al, Ni oxidized to NiS; (2) at > 1.6 V, the electrochemical reaction to form polysulfide anions in the presence of Li_2S, and a slow chemical-exchange reaction between NiS and Li_2S_2 to form NiS_2, occurred.
- ANL has identified two glass compositions (P-glass, 43.1 mol% Na_2O, 8.3 mol% Al_2O_3, 5.5 mol% ZrO_2, and 43.1 mol% SiO_2; X-glass, 40 mol% Na_2O, 12 mol% Al_2O_3, and 48 mol% SiO_2) that exhibited low weight change in Na, Na_2S_4, and S at 400°C. These glasses, which have sodium-ion conductivity of 162 ohm-cm and 484 ohm-cm, respectively, are potentially attractive candidates for use as solid electrolytes in Na/S cells.
- Studies at the University of Pennsylvania on polymer electrolytes have indicated that polyacetylene does not appear to offer major advantages over current electrodes for high-energy-density, rechargeable, nonaqueous electrochemical cells. Polyacetylene has low volumetric energy density and low-moderate gravimetric energy density, and is sensitive to impurities.

Electrochemical Processes

- Pyrolysis gas chromatography–mass spectrometry studies by Case Western Reserve University have indicated that heat-treatment of Co and Fe tetramethoxyphenyl porphyrin at temperatures between 350° and 450°C results in the loss of fragments associated with the methoxyphenyl groups but leaves a significant amount of nitrogen.
- Corrosion tests by ANL to identify improved current collector materials for sulfur electrodes have continued. The corrosion of chromium in sulfur at 350°C follows a parabolic rate law with a rate constant of 1.93×10^{-7} cm/s and forms a single layer of Cr_2S_3. In Na_2S_3, the corro-

sion shows a logarithmic rate dependency and forms a two-layer scale of $NaCrS_2$ and Cr_3S_4. The corrosion rate in Na_2S_3 is less than in sulfur.

- Ford Motor has observed that electrodes produced by flame-spraying a mixture of β''-alumina and molybdenum powders delivered 0.4 W/cm^2 in a sodium heat engine operating at 900°C. An improved performance of 0.51 W/cm^2 was achieved with TiN electrodes, but this performance decreased slowly over a period of 140 hours to 0.34 W/cm^2.

Fuel Cell Research

- Studies at Los Alamos National Laboratory (LANL) on steam-reforming of methanol have suggested that rapid oxygen exchange occurs on the catalyst (Cu-ZnO) surface, at rates that are fast compared to the lifetime of methanol or product species on the surface.
- Two solid-polymer-electrolyte (SPE) fuel-cell test systems were delivered by General Electric to LANL. Tests at LANL of a SPE fuel cell with CO-tolerant anode catalyst showed almost instantaneous recovery of initial H_2/air performance after a 6-hour operation on reformate with 0.17% CO.
- United Technologies Corporation has developed a proprietary electrocatalyst (CSV-11) that showed improved CO tolerance to that of Pt at 100 and 140°C in phosphoric acid.
- The University of Virginia was successful in quenching disorder in a 25 at.% Cr – 75 at.% Pt sample. Previous investigators had reported that it was not possible to retain disorder in samples of this composition.

Program Changes in 1984

Funding support for the following projects was initiated in 1984:

- Research on Materials Relating to the Sodium Heat Engine—Ford Motor Company
- Development of Bifunctional Oxygen Electrodes for Alkaline Metal-Oxygen Rechargeable Cells—Energy Research Corporation
- Investigation of the Mechanism for Capacity Decline in FeS_2 Electrode in Lithium-Iron Sulfide High-Temperature Batteries—Gould, Inc.
- Improve the Lifetime of the Hollow Fiber Sodium/Sulfur Cell—Dow Chemical Company
- Corrosion-Resistant Coatings for High-Temperature, High-Sulfur-Activity Applications—Illinois Institute of Technology

Funding support for the following projects ended in 1984:

- Study of High-Energy Cathodes and Anodes for Molten Salt Batteries—University of Tennessee
- Sulfolanes as Electrolytic Solvents for Rechargeable Lithium Batteries—EIC Laboratories, Inc.
- Iron/Air Battery Development—Westinghouse Corporation
- Bibliography of Convective Transport Correlations—Illinois Institute of Technology
- Supported Liquid Membrane Battery Separator—Castle Technology
- Battery Separator Research—Sandia National Laboratory
- Thermodynamic Framework for Estimating the Efficiencies of Alkaline Batteries—Ohio State University
- An Electrochemical and Morphological Study of the Effect of Temperature on the Restructuring and Loss of Capacity of Alkaline Battery Electrodes—Ohio State University
- Thermal Management of Battery Systems—Gould, Inc.
- Research on Novel Membranes for Lithium Batteries—Case Western Reserve University
- Continuous Organic Electrochemical Synthesis—University of California at Los Angeles

PLANNED ACTIVITIES FOR FY 1985

New initiatives include the following:

- Selections will be made from proposals submitted in response to a Request for Proposals (RFP) issued by the TBR Project on research and development of novel concepts for metal/air batteries.

- Applied research on corrosion in secondary batteries will be conducted.
- Spectroscopic studies of surface films on alkali metals will be performed.

Battery Electrode Studies*†

E.J. Cairns, F.R. McLarnon, J.C. Dobson, R.I. Goldberg, M.J. Isaacson, R. Jain, P.M. Lessner, K.G. Miller, S.A. Naftel, M.L. Smith, K.A. Striebel, and J. Winnick

The purpose of this research is to study the behavior of electrodes used in secondary batteries and to investigate practical means for improving their performance and lifetime. Systems of current interest include ambient-temperature rechargeable cells with zinc electrodes [Zn/air, Zn/NiOOH, Zn/AgO, Zn/Cl_2, Zn/Br_2, and $Zn/Fe(CN)_6^{-3}$]; rechargeable high-temperature cells (Li/S, Li-Al/FeS_2, Li-Si/FeS_2, and Na/S); fuel cells; and liquid-junction photovoltaic cells. The approach used in this investigation is to study life- and performance-limiting phenomena under realistic cell operating conditions.

ACCOMPLISHMENTS DURING FY 1984

The Effect of Electrolyte Species Concentrations on the Cycle-Life Performance of Zn/NiOOH Cells

(M.J. Isaacson, E.J. Cairns, and F.R. McLarnon)

Knowledge of the concentrations and concentration gradients inside a cycling zinc electrode would help researchers to evaluate proposed theories of zinc active material redistribution and identify means to reduce the rate of capacity loss. In order to provide continuous, *in-situ* measurements of electrolyte species concentrations, a system of "microreference electrodes" is being developed for use in model Zn/NiOOH cells. A special cell for measuring the rest potentials of these zinc and cadmium microreference electrodes was built, and equations were developed to calculate KOH and $K_2Zn(OH)_4$ activity coefficients from the rest potentials. Computer programs were then developed for fitting single and binary electrolyte data with Pitzer's equations.[1,2] Pitzer's equations were also used to correlate KOH activity coefficients up to 15 molal. Experimental data were not available for KOH-$K_2Zn(OH)_4$ electrolytes. An algorithm for calculating concentrations inside a cycling porous zinc electrode from the microelectrode potentials, using an activity-coefficient correlation and a model for the liquid-junction potential, was developed.

The Effect of Calcium Hydroxide on Secondary Zinc Electrodes

(R. Jain, E.J. Cairns, and F.R. McLarnon)

The aim of this research is to investigate the addition of calcium hydroxide to the zinc electrode as a practical means of reducing zinc species solubility in strong alkaline electrolytes. The reduced zinc solubility is expected to slow the rate of active material redistribution in the zinc electrode, thereby increasing its cycle life.

Identical pairs of electrodes, containing 0%, 10%, 25%, and 40% $Ca(OH)_2$ by weight, were fabricated and cycled. The Zn electrode containing no $Ca(OH)_2$ was cycled to 100% depth-of-discharge 150 times, and the cell retained over 90% of its original capacity. An x-ray of the electrode showed significant movement of Zn away from the center of the electrode toward the tab side. The 40%-$Ca(OH)_2$ cells shorted within the first few cycles. Analysis indicated that these cells shorted because they could not accept the same charge current density as the $Ca(OH)_2$-free cell. The charge current density for the 25%-$Ca(OH)_2$ cells was therefore adjusted to a value 25% lower than that typically used for $Ca(OH)_2$-free cells. After 100 cycles, the 25%-$Ca(OH)_2$ cells showed some Zn migration to the edges of the electrode, but the capacity remained at 100% of its original value. The 10%-$Ca(OH)_2$ cells were operated for 70 cycles at which point the cells exhibited 60% of their design capacity. Problems with the nickel-oxide electrodes limited the cell capacity to less than 85% of the design value throughout its life. The

*This work was supported by the Assistant Secretary for Conservation and Renewable Energy, Office of Energy Systems Research, Energy Storage Division of the U.S. Department of Energy under Contract No. DE-AC03-76SF00098.

†This project is part of a larger effort, "Electrochemical Energy Storage," described in the *Materials and Molecular Research Division FY 1984 Annual Report* (LBL-18570).

25%-$Ca(OH)_2$ cells also showed problems, albeit to a lesser extent, traced to the NiOOH electrodes. The 10%-$Ca(OH)_2$ cells were able to accept the same charge current density as the $Ca(OH)_2$-free cells, but x-ray analysis of the Zn electrodes after 70 cycles indicated significant Zn redistribution.

Analysis of Zinc Electrode Current Collection in Zn/NiOOH Cells

(R.I. Goldberg, E.J. Cairns, and F.R. McLarnon)

The current collector of the zinc electrode in a Zn/NiOOH cell was modeled as a network of resistors, and the potential and current associated with each node was obtained using a Kirchhoff's current-law analysis. The current flowing across the electrolyte was plotted as a function of position on the current collector.[3] Future experimental work is planned to correlate the calculated current distribution with experimental results to determine the effect of current distribution on cycle life and zinc deposit quality. Design considerations included: placement of tabs, conductivity of the collector as a function of changes in mesh dimensions, and the possibility of enhanced collector function by addition of dispersed conductive material to give a larger area for collection of current.

Mathematical Modeling of the Zinc Electrode

(K.G. Miller, E.J. Cairns, and F.R. McLarnon)

Factors limiting the cycle life of the zinc electrode are redistribution of active material over the face of the electrode[4,5] and passivation[6] (formation of oxide layers over the surface of the electrode). A one-dimensional, time-dependent model is being developed to predict the cause and extent of Zn redistribution and passivation as the electrode is cycled. This model will take into account changes in current density, overpotential, and species concentration.

The equations for the model are being derived and are nearly complete. An exhaustive literature search is being carried out to identify the parameters that must be measured experimentally. Experiments are being set up to measure the electronic conductivity of the zinc electrode at various states of charge and to determine if the electrolyte becomes supersaturated with zinc species during discharge. Both are important in determining the type of model used. Also, the properties of the separator must be measured. These, plus completion of the model, are the immediate goals.

Behavior of Metals in Sulfur-Polysulfide Melts

(J.C. Dobson, F.R. McLarnon, and E.J. Cairns)

To better understand the behavior of various metals for use as current collectors and cell containers in sodium/sulfur and lithium/sulfur cells, two types of studies were performed: (1) cyclic voltammetry in Na_2S_4 and $Li_2S_{3.8}$ (both representative of single-phase polysulfide melt compositions) molten-salt electrolytes at chromium and molybdenum electrodes, and (2) static corrosion tests of molybdenum, chromium, and a 70% Cr–30% Fe alloy in both lithium and sodium polysulfides and molten sulfur. Sodium-polysulfide voltammetry was conducted at 300° and 350°C, and lithium-polysulfide voltammetry at 400°C. The voltammetry experiments employed sweep rates ranging from 5 to 500 mV/sec, and the electrode potentials covered the full range expected in the respective cell systems. The static corrosion tests were performed at 350°C in N_2S_3, 400°C in $Li_2S_{3.8}$, and at both temperatures in molten sulfur. Samples were prepared flat as disks to minimize geometry effects. The samples that were corroded at 400°C were analyzed (after cutting, mounting, and polishing) by SEM, EDAX, and x-ray diffraction techniques; the samples that corroded at 350°C were analyzed by SEM and EDAX methods only.

The design of the cell used in the voltammetry experiments has been described elsewhere.[7] Data from these experiments were compared with sodium polysulfide voltammetry data reported in the literature, which had been gathered using carbon, aluminum, and platinum electrodes. A model was developed to help understand the results of cathodic sweeps in both systems, and the different results for the various metal/melt combinations are explained using thermodynamic and electrochemical arguments.

The data from the static-corrosion studies were compared with reported corrosion mechanisms of the same metals and alloys in sulfur vapor, and the possible influence of solubility of the scale in the melts was measured, as were rate data for the corrosion of the three materials in sulfur and $Li_2S_{3.8}$.

Mathematical Modeling of the Sodium/Sulfur Cell

(S.A. Naftel, F.R. McLarnon, and E.J. Cairns)

Mathematical models of the sodium/sulfur cell[8,9] have been developed, usually to provide improved understanding of the operation of the sulfur elec-

trode. They are one-dimensional and therefore have limited capability to account for phenomena such as convection, which require a two- or three-dimensional framework. Examination of the physical properties[10] of sulfur and sodium polysulfides leads to the conclusion that density and viscosity differences, and preferential wetting,[11] cannot be ignored. The aim of this work is to develop a two-dimensional model of a tubular sodium/sulfur cell that accounts for the actual behavior of an operating cell. In addition to computer modeling, electronic and ionic potential profiles will be measured throughout the cathode via the use of small reference electrodes.

Glass Electrolytes for Lithium/Sulfur Cells

(M.L. Smith, J. Winnick, F.R. McLarnon, and E.J. Cairns)

Several borate glasses have been developed[12] that, upon addition of Li_2O and LiCl, show lithium-ion conductivities as high as $2 \times 10^{-2} ohm^{-1} cm^{-1}$ at 300°C. It has also been observed that the structure of the glasses is maintained in the presence of molten lithium. The aim of this investigation is to construct and operate a Li/S or Li-alloy/S cell that employs a borate fast-ion-conducting glass as the electrolyte.

A successful procedure for making and blowing lithium-chloroborate glass into thin-walled sealed tubes has been developed. These tubes have been tested statically for stability in molten-sulfur/polysulfides at 380°C. A thin white film was observed to form on the glass in the polysulfide melts. The composition of this film and its effect on conductivity are not yet known.

Several electrochemical cells have been constructed using the thin-walled tubes, but each has experienced mechanical failure within a few hours at 380°C. Current work is directed at eliminating the mechanical problems of cell assembly that appear to be causing the failures.

Carbonate Anion Effects on Oxygen Reduction on Platinum in Dilute Alkaline Electrolytes

(K.A. Striebel, F.R. McLarnon, and E.J. Cairns)

Alkaline electrolytes have long been known to support higher oxygen-reduction kinetic currents than those observed in acid electrolytes. However, recent fuel cell work has avoided hydroxide electrolytes because carbonation can occur in the presence of the CO_2 in the hydrogen-rich gas that results from the steam-reforming of carbonaceous fuel. Electrolytes that reject CO_2, such as Cs_2CO_3, were investigated in 1964 by Cairns and Bartosik.[13] This early work demonstrated electrolyte invariance in a methanol/oxygen single cell, where CO_2 is produced at the anode. Overall cell performance was shown to be promising, but no measurements of the oxygen-electrode kinetics were made.

Preliminary kinetic results obtained with the rotating ring-disk electrode technique in dilute Cs_2CO_3 showed higher currents and lower ring currents than KOH at the same concentration, indicating a possible change in reaction mechanism. To study the carbonate-anion effect independently of pH differences, increments of potassium carbonate were added to the well-characterized electrolyte 0.1 *M* KOH. Kinetic currents for three of the electrolytes are shown in Fig. 1. The rise in kinetic current with a series of carbonate additions is shown in Fig. 2. The causes for this behavior have not yet been identified. Ring currents due to peroxide formed at the disk were also found to depend on carbonate concentration. Negligible ring currents (<0.1 μA) were observed in the pure 0.1 *M* Cs_2CO_3 solution (pH = 11.4), whereas significant peroxide was detected in the higher-pH solutions.

Changes in oxygen solubility due to the increase in ionic strength of the solution would result in the

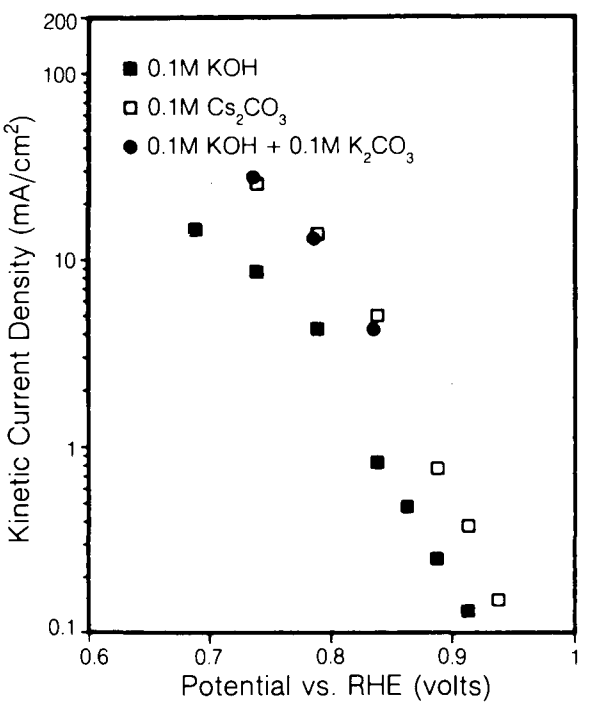

Figure 1. Current-potential behavior for oxygen reduction on platinum in alkaline electrolytes. (XCG 851-39A)

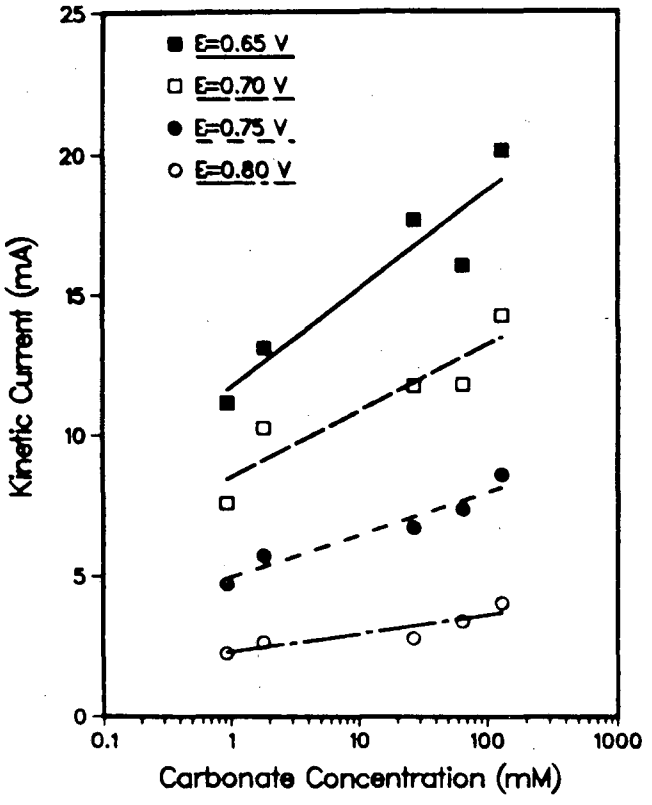

Figure 2. Kinetic currents for oxygen reduction on platinum in alkaline electrolytes containing 0.1 M KOH as a function of carbonate-ion concentration for different potentials. (XCG 851-40)

opposite trend in kinetic currents; however, other effects of the ionic strength are possible.

Future work will focus on determining the reasons for the positive anion effect, as well as its extent. Experiments with more concentrated electrolytes are planned.

Engineering Analysis of Photoelectrochemical Cells

(P.M. Lessner, J. Winnick, E.J. Cairns, and F.R. McLarnon)

Efforts during 1984 have concentrated on producing efficient counterelectrodes for photoelectrochemical cells based on the sulfide/polysulfide redox couple. The sulfide/polysulfide redox couple shows highest exchange current densities on transition metals and transition-metal sulfides such as CuS, MoS_2, and CoS. Our approach has been to disperse these metal sulfides in a hydrophilic carbon matrix in order to maximize surface area. A small amount (~3 w/o) of PTFE was added to bind the electrode together, and the active material was hot-pressed onto an expanded Ni mesh. The electrodes were less than 1 mm thick and had 15 cm^2 of projected area, with an active-material porosity of about 75%.

The electrodes have been tested in a parallel-plate electrochemical cell in which the test electrode and counterelectrode were held about 3 mm apart. A Pt wire between the two electrodes served as a reference electrode. Curves of steady-state current versus electrode polarization were taken for each test electrode. To assist interpretation of the electrochemical data, sections of the electrodes have been examined with the scanning electron microscope and with a powder x-ray diffractometer. To determine the kinetic parameters, transient experiments on smooth metal or metal-sulfide disks are planned.

PLANNED ACTIVITIES FOR FY 1985

Continuing research efforts on secondary alkaline zinc electrodes will focus on the application of *in-situ* microelectrode potential measurements to determine electrolyte species concentrations in operating zinc electrodes; development of a comprehensive mathematical model; the performance of cycle-life experiments to complement mathematical analysis of zinc-electrode current collection; electrolyte and electrode formulations that exhibit reduced zinc-species solubility; and the microscopic study of model zinc electrodes. High-temperature alkali metal/sulfur cell studies will include mathematical modeling of the sulfur electrode and complementary operation of Na/S cells and operation of model Li/glass electrolyte/S cells. Additional research on alkaline electrolytes for fuel cells will continue, as will the fabrication and testing of high-performance sulfur/polysulfide electrodes for use as counterelectrodes in liquid-junction photovoltaic cells.

REFERENCES

1. Pitzer, K.S. and Moyorga, G. (1973), "Thermodynamics of Electrolytes. II. Activity and Osmotic Coefficients for Strong Electrolytes with One or Both Ions Univalent," *J. Phys. Chem. 77*, p. 2300.
2. Pitzer, K.S. and Kim, J.J. (1974), "Thermodynamics of Electrolytes. IV. Activity and Osmotic Coefficients for Mixed Electrolytes," *J. Am. Chem. Soc. 96*, p. 5701.
3. Goldberg, R.I., McLarnon, F.R., and Cairns, E.J. (1984), *Novel Current Collectors for the Zinc Electrode in Zn/NiOOH Cells—Interim Report,* Lawrence Berkeley Laboratory report LBID-984.

4. McBreen, J. (1972), "Zinc Electrode Shape Change in Secondary Cells," *J. Electrochem. Soc. 119*, p. 1620.
5. Choi, K.W., Bennion, D.N., and Newman, J. (1976), "Engineering Analysis of Shape Change in Zinc Secondary Electrodes. I. Theoretical," *J. Electrochem. Soc. 123*, p. 1616; "Engineering Analysis of Shape Change in Zinc Secondary Cells. II. Experimental," *ibid.*, p. 1628.
6. Sunu, W.C. and Bennion, D.N. (1980), "Transient and Failure Analysis of the Porous Zinc Electrode. I. Theoretical," *J. Electrochem. Soc. 127*, p. 2007; "Transient and Failure Analyses of the Porous Electrode. II. Experimental," *ibid.*, p. 2017.
7. Dobson, J.C., McLarnon, F.R., and Cairns, E.J. (1984), "Corrosion of Metals by Sulfur/Polysulfide Melts," 166th Meeting of the Electrochemical Society, New Orleans, Paper No. 110.
8. Jacquelin, J. and Pompon, J.P. (1979), "A Mathematical Model of the Behaviour of the Molten Sodium Polysulfide Electrode," *Power Sources 7*, p. 713, J. Thompson, Ed., Academic Press, London.
9. Breiter, M.W. and Dunn, B. (1979), "Potential Distribution Model for Rechargeable Sulphur-Electrodes in Sodium-Sulfur Cells," *J. Appl. Electrochem. 9*, p. 291.
10. Cleaver, B., Davies, A.J., and Hames, M.D. (1973), "Properties of Fused Polysulfides-I," *Electrochim. Acta 18*, p. 719; "Properties of Fused Polysulfides-II, III," *ibid.*, p. 727.
11. Janz, G.J. and Murphy, R.M. (1979), "Wettability of Some Carbon Surfaces by Molten Sulfur and Polysulfides," *J. Electrochem. Soc. 125*, p. 1605.
12. Button, D.P., Tandon, R.P., Tuller, H.L., and Uhlmann, D.R. (1981), "Fast Lithium-Ion Conduction in Chloroborate Glasses. II. Diborates and Metaborates," *J. Solid State Ionics 5*, p. 655.
13. Cairns, E.J. and Bartosik, D.C. (1964), "A Methanol Fuel Cell with an Invariant Alkaline Electrolyte," *J. Electrochem. Soc. 111*, p. 1205.

ADVANCED THERMAL ENERGY STORAGE RESEARCH

Advanced Thermal Energy Storage Technologies Project*

P.H. Berdahl, V.P. Carey, A.J. Hunt, R.J. Otto, K.S. Udell, and E.J. Cairns

The primary objective of this project is to select and develop innovative thermal energy storage technologies having the greatest promise of satisfying the economic and performance requirements of future energy-supply, energy-conversion, and end-use applications. The following four research areas were pursued in FY 1984:

(1) development of a solid-state radiative heat pump using narrow-bandgap semiconductor materials and capable of heating or cooling an enclosed space by the direct emission or absorption of thermal radiation;
(2) development of a three-phase thermal energy storage module with constant or variable thermal conductance;
(3) study of the dominant and limiting processes associated with the operation of gas-loaded heat pipes to be used in combined thermal storage and transport; and
(4) experimental and theoretical study of the use of microparticles as an advanced medium for heat exchange and catalysis, with emphasis being given to thermochemical storage reactions.

Descriptions of these four research efforts follow.

SOLID-STATE RADIATIVE HEAT PUMP

(P.H. Berdahl, R. Dalven, L. Shaffer, and S. Sanders)

The purpose of this research project is to establish a research basis for the development of a new class of heat pump. This new heat pump would be a solid-state device that accepts input energy in the form of electricity and pumps infrared (heat) radiation across a thermally insulating gap. An important potential application is residential cooling, in conjunction with thermal storage.

Semiconductor materials with direct narrow bandgaps in the range of 0.03–0.25 eV produce equilibrium thermal infrared radiation, an effect that is in large part due to electron-hole recombination. An excess or deficit of infrared radiation, compared with the thermal equilibrium value, can be produced when the electron-hole concentration is varied from its equilibrium value by electrical means. This excess or deficit of infrared radiation is the basis of the solid-state radiative heat pump. Two techniques for varying the electron-hole concentration are of special interest here: (1) electrical bias of a p-n junction to produce carrier injection or, for reverse bias, carrier extraction; (2) the magneto-concentration effect in which orthogonal electric and magnetic fields are used to enhance (or deplete) the concentration of electrons and holes near the semiconductor's surface. The p-n junction technique seems particularly promising for the development of technologically mature devices, while the magneto-concentration effect offers the opportunity for the study of key recombination phenomena in a simpler experimental system.

Accomplishments During FY 1984

For the idealized example of a p-n junction diode with no series resistance, no nonradiative carrier recombination, or other complicating features, the thermodynamic performance of the device as a "radiant refrigerator" has been determined.[1] Figures 1 and 2 show numerical results for the available cooling rates as a function of semiconductor gap energy E_g and coefficient of performance (COP) for situations in which the Carnot (maximum) COP is 10. For Fig. 1, the reverse electrical bias causes carrier extraction from the region of the junction, leading to a diminution in infrared emission compared with thermal equilibrium. At the same time, the diode can still absorb radiation from a nearby object and cool it. For example, a diode at 300 K cooling an object at 273 K with a COP of 2.5 should have an energy gap of about 1.5 kT (0.039 eV) to produce a maximum cooling rate of 0.34 σT^4 = 156 Wm^{-2}. (The *absolute* maximum cooling rate for these conditions is actually larger by a factor of n^2, where n is the semiconductor's index of refraction.[1]) Figure 2 shows the somewhat larger cooling rates available

*This work was supported by the Assistant Secretary for Conservation and Renewable Energy, Office of Energy Systems Research, Energy Storage Division of the U.S. Department of Energy under Contract No. DE-AC03-76SF00098.

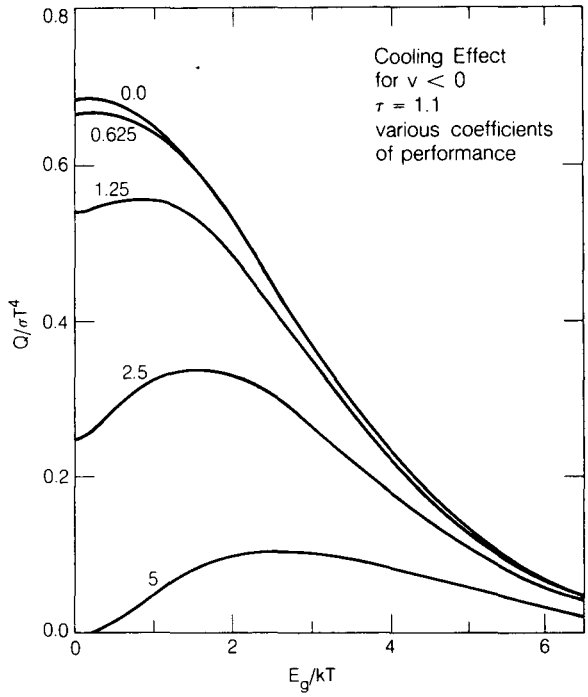

Figure 1. Available radiative cooling effect for a reverse-biased semiconducting diode ($v < 0$), in units of σT^4, where T is the absolute diode temperature and σ is the Stefan-Boltzmann constant. The "external" temperature $T_e = T/\tau$, where $\tau = 1.1$. E_g is the magnitude of the energy gap, and kT equals 0.026 eV at $T = 300$ K.
(XBL 849-8717)

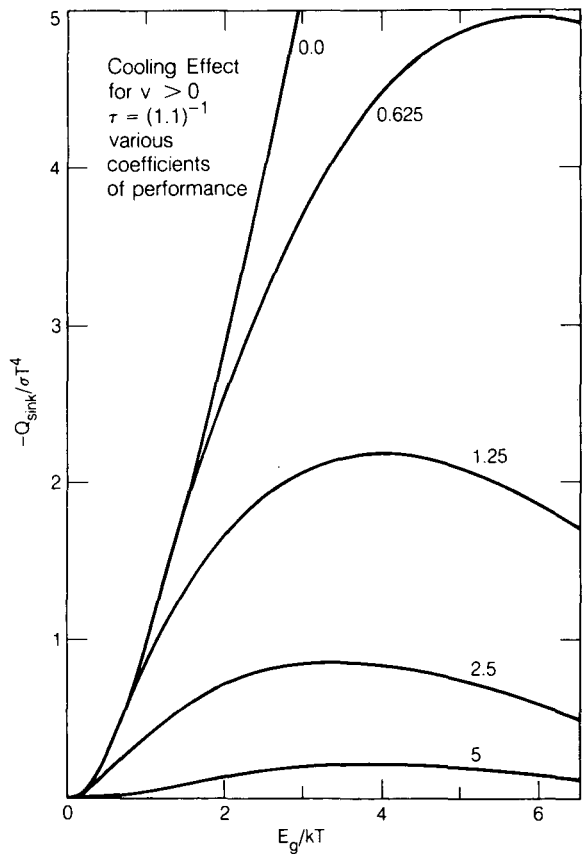

Figure 2. The available radiative cooling effect for a forward-biased semiconducting diode ($v > 0$). The notation is the same as for Fig. 1, except that the cooling effect is now due to the diode emitting more radiant energy than is provided from the input electricity; the (cooling) balance $-Q_{sink}$ is provided from the diode's "heat sink." Here $T_e = T/\tau$, with $\tau = (1.1)^{-1}$. (XBL 849-8716)

with forward-biased diodes in which the diode's heat sink is cooled.

The primary project activity during FY 1984 was the laboratory setup for, and first preliminary measurements of, galvanomagnetic luminescence of indium antimonide (InSb), a semiconductor with a bandgap of 0.18 eV. These measurements will quantify the intensity and spectrum of infrared luminescence due to the magneto-concentration effect. Galvanomagnetic luminescence of intrinsic (pure) InSb was first observed at LBL in July 1984. Several characteristics of the measured radiance allowed unambiguous identification of the phenomenon: the radiance vanishes in the absence of either the electric or the magnetic field. For modulating frequencies of 20 to 200 Hz of the exciting electric field, the observed luminescence is roughly independent of frequency, in contrast with various "ordinary" thermal effects that can contaminate the data and that decrease as the frequency is increased. The spectrum of the radiation has been isolated with filters and found to lie primarily at wavelengths smaller than 7.5 microns, as expected for recombination radiation from InSb.

The intensity of the galvanomagnetic luminescence was found to be roughly 60 μW cm^{-2} in a magnetic field of 0.5 tesla and an electric field of 0.7 V cm^{-1}. This figure is rather uncertain because of to the unknown spectral distribution of the radiation but is reproducible from sample to sample. As expected, the surface condition of the semiconductor is quite important. Chemical etching of the surface is required, since the luminescence from samples that are merely polished to mirror smoothness is weaker by a factor of 4 or 5 than etched samples.

Planned Activities for FY 1985

The galvanomagnetic luminescence measurements with InSb will continue with improved instrumentation. Improvements will include the use of a more sensitive infrared detector, higher magnetic fields, and a grating monochromator to determine

the spectral distribution of the radiation. Samples of p-type InSb will be investigated in addition to intrinsic material.

A new activity to be started in FY 1985 is research toward a proof-of-concept experiment for the solid-state radiative heat pump. A preliminary experiment will utilize the galvanomagnetic luminescence of InSb to demonstrate the existence of a cooling effect (the cooling effect may be masked by various parasitic heating effects). This will be done by placing an object next to an InSb layer in a magnetic field and demonstrating that the equilibrium temperature of the object is lower when current of one polarity is passed through the InSb than when an equal current of the other polarity passes through.

THREE-PHASE THERMAL ENERGY STORAGE MODULE WITH CONSTANT OR VARIABLE THERMAL CONDUCTANCE

(V.P. Carey)

The overall objectives here are to demonstrate the feasibility of a new three-phase storage module concept and to study the energy storage and thermal control mechanisms of the module. The proposed work will examine the module both as a closed uncontrolled storage device and as an actively controlled system. These results will be used to determine optimal module configurations, phase-change materials (PCMs), working fluids, and thermal control techniques for typical storage applications.

To assess the viability of the module concept and investigate thermal transport inside it, a fully instrumented laboratory-scale storage module is being fabricated. This experimental system will use encapsulated Glauber's salt as the PCM and R-11 fluorocarbon as the working fluid. The salt will change phase at 89°F. At this temperature, the vapor pressure of R-11 is about 19 psia, so the test module will operate at just slightly above atmospheric pressure. Experiments will attempt to measure heat transfer during the heat input and extraction processes and the storage capacity of the system.

Accomplishments During FY 1984

During the past year, the prototype laboratory-scale storage module was designed, and fabrication was started in the shop. The fabrication and assembly of the apparatus are nearly complete. The PCM salt and R-11 fluorocarbon fluid for the module have been procured.

Planned Activities for FY 1985

By early February 1985, we plan to have the prototype module assembled and ready for testing. Testing of the unit is expected to continue into June 1985. In parallel with our testing, we are working on an analytical model of thermal transport in the module. By the end of June 1985, we expect to have demonstrated the feasibility of the module concept and to have sufficient data to test the analytical model.

GAS-LOADED POROUS HEAT PIPES FOR ENHANCED CONDUCTANCE AND INTEGRATED THERMAL ENERGY STORAGE CONTROL

(K.S. Udell)

Recent work[2] has shown that under certain thermodynamic conditions, a porous medium saturated with a wetting liquid and its vapor will exhibit an apparent thermal conductivity several orders of magnitude larger than metals such as copper. These high conductivities result from capillary-driven flows analogous to the operation of heat pipes. By combining porous media of two different permeabilities, enhanced wicking limits and higher heat fluxes than those of homogeneous media can be maintained.[3] Because inexpensive porous materials such as silica sand can be used in producing this high-conductivity system, the "porous heat pipe" is of particular interest for use in thermal energy storage. Furthermore, phase-change materials can be accommodated within the porous structure without serious degradation of heat-transfer performance. Nevertheless, research must be performed on topics involving the thermodynamics of phase change in porous media and the effect of noncondensables on the performance of porous heat pipes before specific designs can be optimized.

Accomplishments During FY 1984

During the initial funding period (July–September 1984), a capillary pressure probe was developed that will be used to diagnose the operation of experiments involving the heat pipe effect in porous media. An apparatus for studying the thermodynamics of phase change in porous media was fabricated and yielded encouraging preliminary results. A dual-permeability porous heat pipe was built for experimental studies, and prelim-

inary modeling of the effect of noncondensables on performance was conducted. Finally, software was developed for a computerized data acquisition system that will be needed in support of the experimental effort.

Planned Activities for FY 1985

Studies of the thermodynamics of phase change in porous media are planned. A one-dimensional, steady-state model of the effect of noncondensables on porous heat pipe performance will be completed and experimental verification initiated. The concept of the dual-permeability porous heat pipe will be examined experimentally.

MICROPARTICLES AS ADVANCED MEDIA FOR HEAT EXCHANGE AND CATALYSIS

(A.J. Hunt, P. Hull, R.J. Otto, F. Miller, and J. Ayer)

The objective of this research is to investigate potential thermochemical storage reactions of gases at the surface of suspended particles in the presence of sunlight. The main tasks are to survey candidate reactions for this application and to initiate an experimental study of the effects of sunlight on one or two selected reactions.

Accomplishments During FY 1984

A survey of the literature, including journal articles, technical reports, and conference proceedings, was made in order to compile a list of chemical cycles suitable for the storage of thermal energy using irradiated small particles. These thermal storage cycles generally consist of two (or more) steps: (1) an endothermic step in which energy is supplied to decompose a compound and (2) an exothermic step in which the products of the decomposition are recombined to provide useful heat. Of particular interest were cycles in which the endothermic step could be adapted to a small-particle, direct-flux solar reactor such as the STARR (Solar Thermally Activated Radiant Reactor).

The STARR uses extremely small particles, generally less than 1.0 μ in diameter, as the solar flux absorber and heat exchanger. In some reactions, however, the particle may also act as a catalyst or as the material to be decomposed. The compound that is to be decomposed in the endothermic step may be in the gas, solid, or liquid phase, and it is convenient to divide the reactions into three classes based on the state of the initial reactant.

(1) *Gas-phase reactants.* The absorber particles are entrained in the gas and the mixture is passed through the concentrated solar flux. The particles absorb the solar energy and rapidly transfer this energy to the gas, raising it to the high temperature necessary for the reaction. The particles may play one or both of two roles. In the simpler role, the particle material is chemically inert to the reactant gas and passes through the receiver, acting only as an absorber and heat exchanger. In the second role, the particle material is also a catalyst for the reaction as well as the absorber and heat exchanger. This case offers the potential for some interesting and innovative "photo-assisted" reactions. The SO_3 dissociation reaction using hematite (Fe_2O_3) as catalyst is an example of a reaction that will fit the above description.

(2) *Solid-phase reactants.* If the reactant material is a good absorber over the solar spectrum and can be reduced to a fine powder, it can be entrained in a nonreacting gas and act as the absorbing particle as well as the feedstock for the reaction. Reactions involving compounds of this kind are especially attractive for the STARR if the particle/reactant is commercially available as a fine powder at a reasonable cost. An example of a candidate reaction in this category is the decomposition of $Ca(OH)_2$ to form calcium oxide and water.

(3) *Liquid-phase reactants.* This case requires an extra step in which the liquid is converted to vapor and processed as in the first class of reactions (gas-phase reactants). An example of reactions in this category would be the decomposition of methanol to hydrogen and carbon monoxide.

The decomposition of sulfur trioxide was chosen as the initial reaction to investigate the feasibility of the STARR concept for thermochemical energy storage. This reaction has several advantages: it has a relatively large endothermic enthalpy of dissociation, both SO_2 and SO_3 can be stored as liquids at or near ambient temperature, and there has been an extensive evaluation of a thermochemical storage cycle using this reaction.[4] One catalyst for the SO_3 dissociation reaction is hematite (Fe_2O_3). The hematite is a good adsorber of solar radiation and is readily available as small particles in the 0.5 to 1.0 μm-size range. The primary goal of the experimental part of this project is to demonstrate that solar-irradiated small particles can serve to transform the solar flux into high-temperature thermal energy and at the same time catalyze the reaction. At a gas tem-

perature of 850°C, about 90% of the SO_3 is dissociated. Temperatures in this region have been obtained in tests with carbon particles using the SPHER (Small Particle Heat Exchange Receiver).

Particle-assisted photodissociation of SO_3 using solar-irradiated small particles as a catalyst may also be possible. The reactor and experimental procedure will be designed to include the capability of detecting photodissociation-induced shifts in the predicted SO_2SO_3 equilibrium ratio. Figure 3 illustrates the effect on the equilibrium position being sought experimentally. The percent of SO_3 dissociated versus temperature is plotted for an initial SO_3 pressure of 1 atm. At a given temperature, and for all possible reaction mechanisms, the percent of SO_3 dissociated cannot exceed the thermodynamic limit and must lie on or below the curve in the shaded region. The experimental results obtained by Rocket Research Co.[5] using Fe_2O_3 illustrate this rule. However, it is possible to photodissociate SO_3 at room temperature, using UV light. At sufficiently high UV-flux densities, the degree of dissociation can be maintained at a level exceeding the equilibrium value. In this case, the SO_3 molecule directly absorbs a photon with energy exceeding that required for dissociation. The enthalpy of dissociation for SO_3 is 25 kcal/mole or 1.1 eV/molecule. Thus solar photons contain sufficient energy for the dissociation process if there is a mechanism to transfer the photon energy directly into the SO_3 molecule. This

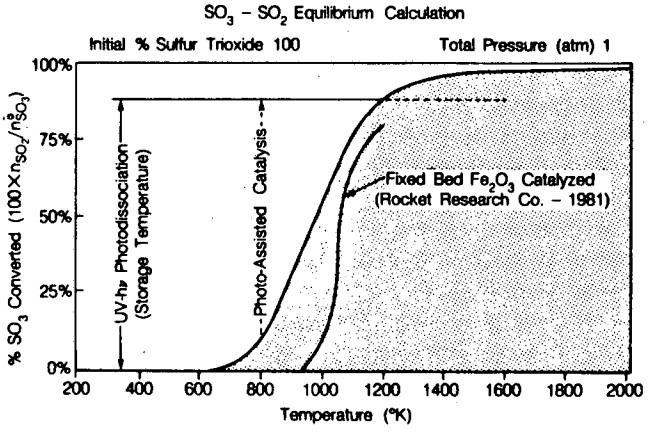

Figure 3. Calculated equilibrium distribution for the reaction $SO_3 \rightarrow SO_2 + \frac{1}{2} O_2$ as a function of temperature. The arrow labeled "UV-hν Photodissociation" highlights a known room-temperature process. The dotted arrow represents an unproven process that is being sought in the project. The experimental results of Rocket Research Co. with a fixed-bed hematite catalyst are shown as a solid curve below the calculated equilibrium curve.

(XBL 853-1888A)

could provide a degree of dissociation exceeding the apparent equilibrium value at a given temperature. An SO_3/SO_2 storage system capable of utilizing solar photons directly and operating at lower temperatures would have a greater efficiency, reduced capital costs, and increased lifetime over a system based on thermal equilibrium.

A number of possible mechanisms for particle-assisted photodissociation of SO_3 were considered. One mechanism would produce reduced sites on the surface of the Fe_2O_3 particles by photodissociation of the hematite. Upon contact with SO_3 these reduced sites would recover the lost oxygen, releasing SO_2 and being restored to their original state. This mechanism is consistent with the high-temperature, thermally induced mechanism for Fe_2O_3 catalysis proposed by Rocket Research Co. Other possible mechanisms include the production of electron-hole pairs and their combined oxidation-reduction of SO_3 leading to dissociation. Hematite does have semiconductor properties with a bandgap of 2.2 eV.

Planned Activities for FY 1985

Work will continue on the primary objective, demonstrating the capability of the solar-irradiated particles to be both heat exchanger and catalyst. Experiments will include high-temperature (850°C) light and dark reaction of gas-phase SO_3, using a method for simulating particles suspended in the gas. The simulation technique involves the dispersion of particles on a nonreacting quartz disk. The particles are widely spaced to eliminate diffusion-dominated kinetics. The reactor will have a fixed volume to allow the system to come to its equilibrium concentration of SO_3, SO_2, and O_2. The experimental design also includes a search for particle-assisted photodissociation of SO_3. A solar simulator capable of providing an equivalent solar intensity of 5000 suns will be used for this phase of the work. The study of suspended-particle heat exchange and catalysis in the solar simulator, using a flowing particle/gas stream, will also be initiated.

REFERENCES

1. Berdahl, P. (1984), *Radiant Refrigeration by Semiconductor Diodes,* LBL-18601.
2. Udell, K.S. (1985), "Heat Transfer in Porous Media Considering Phase Change and Capillarity—The Heat Pipe Effect," *Int. J. Heat Mass Transfer,* in press.
3. Udell, K.S. and Jennings, J.D. (1984), "A Composite Porous Heat Pipe," in Proceedings of the

5th International Heat Pipe Conference, Tsukuba, Japan, May 1984.

4. Dayan, J., Lynn, S., and Foss, A. (1979), *Evaluation of a Sulfur Oxide Chemical Heat Storage Process for a Steam Solar Electric Plant*, LBL-7868.

5. Schmidt, E.W. (1980), "Development of A Long-Life High Temperature Catalyst for the SO_2/SO_3 Energy Storage System," Rocket Research Co., Report RRC-80-R-697.

This report was done with support from the Department of Energy. Any conclusions or opinions expressed in this report represent solely those of the author(s) and not necessarily those of The Regents of the University of California, the Lawrence Berkeley Laboratory or the Department of Energy.

Reference to a company or product name does not imply approval or recommendation of the product by the University of California or the U.S. Department of Energy to the exclusion of others that may be suitable.

LAWRENCE BERKELEY LABORATORY
TECHNICAL INFORMATION DEPARTMENT
UNIVERSITY OF CALIFORNIA
BERKELEY, CALIFORNIA 94720